The fibrosis progression, and treatment of the *NCU-G1*$^{gt/gt}$ mouse model

Camilla Schjalm

Master thesis in Molecular Biosciences

Programme option: Biochemistry

Department of Biosciences

The Faculty of Mathematics and Natural Sciences

University of Oslo

June 2013

There is nothing like looking, if you want to find something. You certainly usually find something, if you look, but it is not always quite the something you were after.

J.R.R. Tolkien

The Hobbit 1937, chapter 4 (Thorin)

Preface

This thesis is the finishing work of a Master's degree in biochemistry. The work was carried out for the Eskild group at the Program for genetics, gene-regulation and gene-function (Gene-program,) at the Department of Biosciences, University of Oslo.

I want to thank all the members of the Eskild group for supporting me through the thesis and giving me the guidance and motivation I needed to finish my degree. I have received good support and been given leeway to think and develop on my own.

Thanks to Professor Winnie Eskild for her guidance and for giving me the possibility to grow independent in the field under her supervision. I also want to thank her for allowing me to experience both the national and international research society.

I want to thank Mc.Sci Xiang Yi Kong especially for the patience, guidance and long laboratory hours he have endured by my side. Your help is invaluable.

A huge thanks to my family for always supporting me and for listening no matter how far down the rabbit hole my rambling of livers and mice went. I also want to thank you for being there for me and each other through the ups and down in life, I love you always.

Thanks to my friends for all the support I have received, from long lunches with jabbering to acceptance of social withdrawal. Also a thanks to study-mates who have been struggling there own fights by my side. We are finally there.

Last, but not least, William, you give me the support and understanding I can only get from you. Thanks for being who you are, and for being mine. I will give you all the support you need to finish your thesis.

Oslo 01.06.3013

Camilla Schjalm

Abstract

Hepatic fibrogenesis is a wound healing response to continuous or chronic insults to the liver. The fibrotic stimuli are often based on disease, genetic disorders, abuse of alcohol and drugs or physical injury to the liver. The stimuli activate hepatic stellate cells (HSC) and other fibrogenic cell types, which induce up-regulation of the expression of pro-fibrotic factors and extracellular matrix (ECM) components leading to an alternated ECM. The matrix metalloproteinases (MMPs) and their inhibitors tissue inhibitors of metalloproteinases (TIMPs) are the main ECM remodelers, and an imbalance in their expression may lead to fibrosis. If left untreated, it may develop to its severe form, cirrhosis. Liver fibrosis is a dynamic process that can be reversed both spontaneously, by removal of the causative agent, and therapeutically by the aid of anti-fibrotic drugs.

NCU-G1 (kidney predominant protein) is a protein consisting of 404 amino acids, in mice, with a predicted molecular weight of 43.8 kDa. It is highly conserved among species. *Ncug1* is highly expressed in liver, kidney and prostate. NCU-G1 has been shown to be a nuclear protein functioning as a co-activator for peroxisome proliferator activated receptor α (PPAR-α), and a higly glycosylated lysosomal membrane protein. A *NCU-G1*$^{gt/gt}$ mouse has been developed, and it is shown to successfully lack the expression of *Ncug1*. The *NCU-G1*$^{gt/gt}$ mice are fertile and grow normally, but spontaneously develop liver fibrosis.

This study investigates the fibrosis progression in the *NCU-G1*$^{gt/gt}$ mice with gene expression, protein and liver component analyses. A pilot study was conducted to investigate the applicability of the *NCU-G1*$^{gt/gt}$ mice as a fibrosis model organism, with treatment with the anti-fibrotic agent sodium hydrogen sulfide (NaHS).

The fibrosis in the *NCU-G1*$^{gt/gt}$ mice liver increase until the mice reaches 4.5 months of age, after 4.5 months the fibrotic state revert to some degree. Treatment with NaHS attenuated the fibrotic state to some degree in the *NCU-G1*$^{gt/gt}$ mice.

Contents

List of Figures

List of Tables

Abbreviations

α-SMA	α-smooth muscle actin
Bcl-x_L	B-cell lymphoma-extra large
BDL	Bile duct ligation
CBS	Cystathionine β-syntase
CCl_4	Carbon tetrachloride
CNS	Central nervous system
Col1α1	Collagen type I α 1
CSE	Cystathionine γ-lyase
Ct	Cycle threshold
ECM	Extracellular matrix
ET-1	Endothelin-1
EtBr	Ethidium-bromide
HCC	Hepatocellular carcinoma
HCV	Hepatitis C virus
HRP	Horse radish peroxidase
HSC	Hepatic stellate cells
IP	Intraperitoneal
KC	Kupffer cells
KO	Knock out
LAMP	Lysosomal-associated membrane protein
LC3	Microtubuleassociated protein light chain 3
LPS	Lipopolysaccharide
LSD	Lysosomal storage disease
MCP-1	Monocyte chemotactic protein-1
MIP-2	Macrophage inflammatory protein-2
MMP	Matrix metalloproteinase
MT-MMP	Membrane-type matrix metalloproteinases
NaHS	Sodium hydrogen sulfide
NK	Natural killer
PCR	Polymerase chain reaction
PDGF	Platelet-derived growth factor
PPAR	Peroxisome proliferator activated receptor
PSC	Primary sclerosing cholangitis

qRT-PCR	Quantitative real time-PCR
ROS	Reactive oxidative species
RT	Reverse transcriptase
S100A8	S100 calcium binding protein A8
SDS-PAGE	Sodium dodecyl sulphate polyacrylamide gel electrophoresis
TAA	Thioacetamide
TGF-β1	Transforming growth factor-β1
TIMP	Tissue inhibitors of metalloproteinase
TNF-α	Tumor necrosis factor α
TRAIL	Tumor necrosis factor-related apoptosis-inducing ligand
VEGF	Vascular endothelial cell growth factor
WT	Wild type

Chapter 1

Introduction

Hepatic fibrogenesis is a wound healing response to continuous liver insults. The liver damage activates hepatic stellate cells (HSC) and other hepatic fibrogenic cell types, leading to an imbalance between the synthesis and degradation of extracellular matrix (ECM) in the liver [1, 2].

Activation leads to an increase in synthesis of ECM, and the main components of the ECM are altered from collagen IV to collagen type I and III, and other fibrotic components such as laminin and fibronectin [1, 3].

The progression of fibrosis is due to the inability of the matrix metalloproteinases (MMPs) which degrade ECM, to keep up with the synthesis of ECM by the HSC. This is mainly due to the altered expression of the MMPs, and an increased expression of the tissue inhibitors of metalloproteinases (TIMPs) [1].

1.1 Liver fibrosis

Fibrosis is the formation of scar tissue by accumulation of ECM after liver injury. The "normal" ECM in the subendothelial space of Disse contains low-density type collagen IV which is replaced with fibril forming collagens I and III (figure 1.1) during fibrosis progression.

The formation of scar tissue forms septae and broad bands of scar-encircled nodules of hepatocytes, which leads to alteration of the liver structure during fibrosis. The changes in pathology can lead to portal hypertension, decreased metabolite flow and impaired liver function [1] .

The fibrosis will, if untreated or reversed, develop into cirrhosis. Severe cirrhosis is difficult to treat, and will often lead to severe pain and eventually death

of the patient. There is an elevated risk for developing hepatocellular carcinoma (HCC) which is shown to increase the rate of mortality in patients with cirrhosis [4].

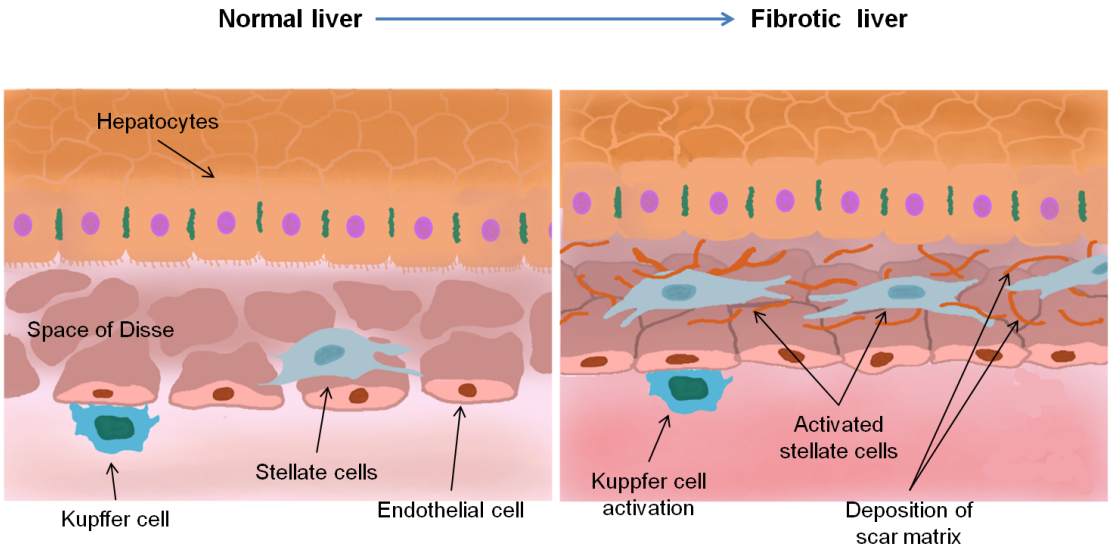

Figure 1.1: **Formation of scar tissue in space of Disse.** During the progression of fibrosis the normal liver extracellular matrix composition changes, and the cellular composition alters with the activation of stellate cells and Kupffer cells. These cells secrete chemokines and cytokines such as transforming growth factor β, endothelin-1 and platelet-derived growth factor, which in turn lead to recruitment of inflammatory cells and the activation of more stellate cells. The activated cells alter their gene expression and the normal extracellular matrix is replaced with scar (fibril-forming) matrix such as collagen I and II. Figure modified from [5]

1.2 The fibrogenic cells

The liver is composed of many different cell types such as HSC, hepatocytes, Kupffer cells (KC) and endothelial cells, and some of them play important roles during the development of fibrosis. The cells that collaborate in the development of fibrosis are termed fibrogenic cells. The main purpose of the fibrogenic cell response is to repair damage to the liver and restore normal liver function [6].

1.2.1 Liver specific fibrogenic cells

HSC has been shown to be the major fibrogenic cell type [7]. In normal liver HSC are vitamin A storing cells that are residents of the space of Disse. The mechanism of HSC activation appears to be disease-specific [8] but the fundamental characteristics of activation are similar in most cases [7].

The first step of activation is initiation by paracrine stimuli like oxidative stress, apoptotic fragments and cytokines from damaged neighboring liver cells and infiltrating inflammatory cells. The HSC become responsive to cytokines, and this initiates scar formation [6].

After initiation HSC activation continues with perpetuation of the activation in seven different steps. (1) The cells proliferate under the influence of mitogenic cytokines such as platelet-derived growth factor (PDGF) [9], vascular endothelial growth factor (VEGF), fibroblast growth factor and thrombin [10]. (2) The HSC, in the space of Disse, accumulate to the site of inflammation because of migratory and chemotactic signals from cytokines such as transforming growth factor $\beta 1$ (TGF-$\beta 1$), endothelin-1 (ET-1) and PDGF [11], Rho signalling [12] and altered interactions in the cell matrix [13]. (3) One of the main drivers of fibrogenesis is the cytokine TGF-$\beta 1$. The production and activation of TGF-$\beta 1$ and its receptor are enhanced in the HSC, and the expression of TGF-$\beta 1$ pseudoreceptor is down-regulated. This contributes to the amplification of TGF-$\beta 1$ activity in the fibrotic liver [14]. (4) The accumulation of inflammatory cells is further increased by the HSC release of pro-inflammatory, pro-fibrogenic and pro-mitogenic cytokines such as monocyte chemotactic protein-1 (MCP-1) and macrophage inflammatory protein-2 (MIP-2) [15, 16]. This inflammatory cell accumulation stimulates the production of ECM by HSC through autocrine pathways such as the TGFβ and PDGF pathway [17]. (5) The cells become more contractile leading to reduced blood-flow in the sinusoids, thereby contributing to increased portal pressure in the damaged liver. ET-1, which is a potent vasoconstrictor, is a key component in this response [18]. (6) The normal liver matrix is degraded, which disrupts the scaffolding in the liver and impairs liver function [19]. (7) The HSC loose their vitamin A droplets and their ability to respond to retinoid receptor signalling [20].

The HSC interact directly with KC during activation, and they activate T-cells and stimulate lymphocyte proliferation by displaying features of professional antigen presenting cells (figure 1.2) [21]. HSC express Toll-like receptors and secrete chemokines when stimulated by Toll-like receptors ligands like lipopolysaccharide

(LPS), flagellin and double-stranded RNA [22, 23]. The HSC are susceptible to natural killer (NK) cell-mediated attack when they are activated and they are cleared from the tissue by NK cells during resolution of fibrosis [24].

Several cell types other than HSC are active during the fibrogenesis. KC are resident macrophages in the lumen of the liver sinusoids. They play an important part in HSC activation, and release a variety of inflammatory mediators, ECM proteinases, free radicals and fibrogenic cytokines during the early stages of liver injury [25].

Hepatocytes in the liver are targets of hepatic pathogens and hepatoxic agents, and can act as antigen presenting cells thereby provoking immune responses. If the hepatocytes are injured they will activate the HSC and recruit inflammatory cells by releasing reactive oxidative species (ROS)-, inflammatory-, and fibrogenic mediators, and apoptotic bodies [26].

Liver endothelial cells play a role in the activation and progression of fibrosis. Sinusoidal endothelial cells produce a splice variant of cellular fibronectin (EIIIA isoform) which activates HSC [27]. They synthesize type IV collagen and laminin, and produce ET-1 which makes the HSC more contractile and regulate the blood-flow in the liver [28]. Bile duct epithelial cells produce pro-fibrogenic cytokines such as TGF-β1, PDGF and connective tissue growth factor which stimulate myofibroblast activation during some liver injury conditions [29, 30].

Epithelial cells are able to transdifferentiate, forming fibroblasts, following morphogenic pressure from injured tissue by epithelial-mesenchymal transition, which is induced by cytokines associated with proteolytic digestion and inflammation like TGF-β1 and MMPs [31].

1.2.2 Recruited cells

There are other ECM producing cells besides the liver specific fibrogenic cells during liver injury, and some of them originate from other tissues. Different subpopulations of mesenchymal cells [32] and cells with hematopoietic origin [33], can be recruited depending on the type of injury inflicted on the liver.

Immune cells play an important role in the progression and resolution of fibrosis. T and B lymphocytes are both implicated in hepatic fibrosis by interaction with other key fibrogenic cells and the cytokines they release [34]. B cells may interact with fibrolytic pathways during the resolution of fibrosis by influencing the

deposition of collagen in the liver [35]. NK cells are important for killing activated HSC [36], leading to removal of the fibrogen producing cells [37], and they are able to recruit T-cells and other immune cells to resolve the liver fibrosis [24, 36, 38].

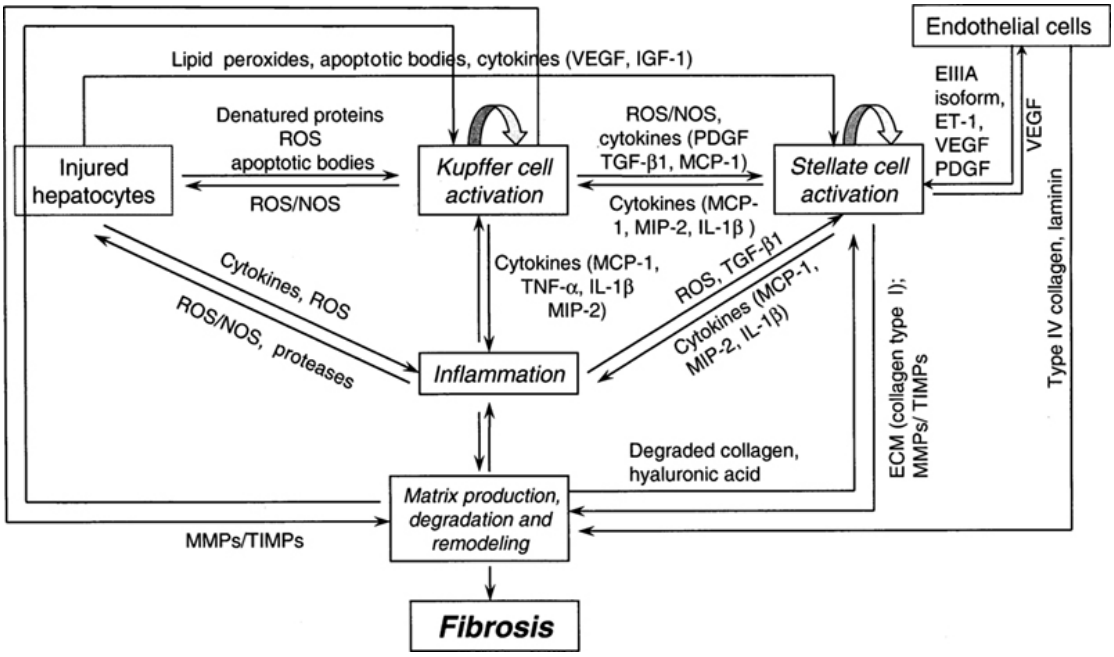

Figure 1.2: **Regulation of fibrosis development.** The network of liver cells, cytokines and extracellular matrix components interplay during the development of liver fibrosis. ECM; extracellular matrix, VEGF; vascular endothelial growth factor, IGF; insulin like growth factor, ROS; reactive oxygen species, PDGF; platelet-derived growth factor, TGF-β1; transforming growth factor-β1, MCP-1; monocyte chemotactic protein, NOS; nitric oxide species , MIP-2; macrophage inflammatory protein-2, IL-1β; interleukin-1β, TNF-α; tumor necrosis factor-α MMP; matrix metalloproteinases, TIMP; tissue inhibitors of metalloproteinases, ET-1; endothelin-1. Figure modified from [1]

1.3 Pathogenesis

The type of stimulus leading to fibrosis is often based on disease, abuse of food and/or alcohol, injury or genetic disorders, and the type of stimuli will influence the fibrosis development. The fibrotic ECM producing cells react to factors such as hypoxia, oxidative stress, immune-responses and apoptosis [1]. The activation

of HSC leads to up-regulation of several pro-fibrotic factors such as TGF-β1 [6], PDGF [9] and tumor necrosis factor α (TNF-α) [39], and to the imbalance between ECM synthesis and degradation [1].

1.3.1 Hypoxia

Hypoxia in the liver is considered a serious fibrotic inducer and often originates from defects in the organ's metabolite delivery system, such as capillarization of the sinusoids and intrahepatic shunting [40], injury to the liver by compression from inflammation and thrombosis, or continuous challenging with drugs or alcohol which leads to raised metabolic demands [41].

Hypoxia will influence the function of the mitochondria which in turn will induce oxidative stress to the liver [1]. Hypoxia induces the HSC to synthesize collagen I by up-regulating genes such as hypoxia-inducible factor 1 alpha which induces the VEGF and its receptors [42–44]. TGF-β1 expression is enhanced by hypoxia in HSC and KC [45], and drives the synthesis of fibrotic ECM [45].

Fibrosis itself is an inducer of hypoxia turning the development of fibrosis from hypoxia into a vicious circle. The conditions enhance each other and can drive the progression of fibrosis into cirrhosis [1].

1.3.2 Oxidative stress

Oxidative stress may initiate fibrosis through induction of liver damage resulting in a number of cellular responses. Damage to the mitochondria will lead to leakage of reactive oxidants such as O_2, H_2O_2, $^{\cdot}OH$, $RO^{\cdot}$ $ROO^{\cdot}$ and $ONOO^{-}$, which are the reactive species in oxidative stress.

ROS damage the bonds in DNA, proteins and lipids in the inner and outer membranes of cells leading to apoptosis and necrosis of parenchymal and non-parenchymal cells. This again may lead to inflammatory responses which initiate fibrosis [1].

HSC, KC and other inflammatory cells are influenced by ROS and react by synthesizing pro-fibrogenic mediators such as TGF-β1, α-smooth muscle actin (α-SMA), resistin-like molecule-α, MMPs, and TIMPs [46,47]. These factors influence the inflammatory response and further activation of HSC. HSC are stimulated to proliferate by ROS, enhancing the response to ROS in the liver [48].

In liver samples from patients with chronic liver disease ROS, lipid peroxidation

products, protein and carbohydrate oxidation products, reactive nitrogen species and products from oxidative DNA damage are often detected [49, 50].

1.3.3 Immune-response and inflammation

KC are resident macrophages which, together with the HSC, are essential initiators of the immune response in the liver during fibrosis [15, 51]. Damaged KC, HSC and hepatocytes induce inflammation and recruit inflammatory cells from the innate (NK cells and macrophages) and adaptive (T and B cells) immune system [52]. The immune response is important for several functions that are beneficial or detrimental for the development of fibrosis. The immune-system eliminates harmful pathogens, kills infected cells, regulates the inflammatory cells, recruits and activates myofibroblasts, and regulates the recovery of fibrosis in the liver [24, 34].

Autoimmune diseases like primary biliary cirrhosis, autoimmune hepatitis and primary sclerosing cholangitis (PSC) are known to induce fibrosis in humans [53, 54], but other diseases that compromise the immune system may also induce fibrosis. Bacterial infections that influence the liver, such as intestinal bacterial overgrowth and increased bacterial translocation of gut flora into the blood stream, are inducers of fibrosis by provoking an immune response [55]. Elevated levels of bacterial LPS are detected in several types of chronic liver diseases [56]. Some viruses offset an immune response which leads to fibrosis, the most prominent being hepatitis C virus (HCV) [57, 58], but some types of herpes-virus and other viruses can induce fibrosis in different organs as well [59, 60].

1.3.4 Apoptosis and necrosis

Apoptosis (i.e. programmed cell death) is a fibrotic stimulus by being pro-inflammatory and by influencing gene expression of cells that engulf the apoptotic bodies. HSC up-regulate their expression of collagen I, TGF-β1, α-SMA and produce ROS, while KC secrete TNF-α, Fas ligand and other death ligands after they engulf apoptotic bodies [26, 39, 61].

Necrosis differs from programmed cell death. Cells that die by necrosis lose the integrity of their cell membrane which eventually ruptures, and release cell material and cell-death products into the intracellular space [62]. This leads to an inflammatory response and triggers many of the same cell responses as apoptosis,

leading to induction of fibrosis [63].

Necrosis and apoptosis can be induced by treatment with hepatotoxic agents like carbon tetrachloride (CCl_4), which induces the hepatocytes to express TNF-α [64]. Tumor necrosis factor-related apoptosis-inducing ligand (TRAIL) is a hepatotoxic agent presently regarded as a promising anti-tumor agent, by inducing apoptosis exclusively in tumor cells without influencing healthy tissue. When TRAIL were tested on tissue samples from patients challenged with fibrotic agents, such as steatosis or HCV infection, TRAIL induced massive apoptosis in the fibrotic liver. This poses an important issue when treating patients with liver damage with agents against other diseases [65].

Clearance by apoptosis of the activated HSC is important for reversion of liver-injury [36]. The number of ECM producing cells expressing TIMPs are decreased, the MMPs are not inhibited to the same extent and the clearance of fibrotic compounds by degradation can surpass the synthesis [66].

1.3.5 Steatosis

Steatosis is not a direct fibrosis inducer, but a condition that will make the liver more prone to initiation of fibrosis by other pro-fibrotic factors such as up-regulation of TNF-α, mitochondrial dysfunction and oxidative stress [67].

The development of steatosis arises from mitochondrial dysfunction, insulin resistance, type 2 diabetes, central adiposity and obesity [68], and is commonly associated with alcohol abuse or other metabolic disorders [68,69]. Alcohol abuse, and other metabolic disorders, have been shown to induce steatosis by diminishing the rate of lipid oxidation and enhancing the synthesis of hepatic fatty acid triglycerides and phospholipids. This leads to accumulation of lipids in the cells and the development of a fatty liver [67, 70], thus increasing the risk of cellular dysfunction and cell death [71, 72].

Both alcoholic steatohepatitis, the most serious state of alcoholic liver disease, and non-alcoholic steatohepatitis, the most extreme form of non-alcoholic fatty liver disease, are major diseases developed from steatosis and represent an increasing problem worldwide [67, 68, 73].

1.4 Fibrotic tissue remodeling

The activation of HSC leads to the up-regulation of both the MMPs and their inhibitors the TIMPs. The MMPs are a family of zinc-containing endopeptidases which are calcium dependent and structurally and functionally similar [74]. There are 23 different forms of MMPs in both humans and mice, most of which share orthology among vertebrates [75], and they are divided into 6 groups(table 1.1).

The collagenase group, MMP-1, MMP-8 and MMP-13, cleave collagen I, II and III, and digest certain other ECM proteins. The gelatinases MMP-2 and MMP-9 mainly digest, the denatured form of collagen, gelatine [76]. It has been reported that not only denatured, but also native type I collagens could be degraded by MMP-2 [77, 78]. MMP-3, MMP-10 and MMP-11 are the stromelysins which digest ECM components such as fibronectin and collagen IV. The matrilysins, also called the minimal-domain MMPs because they lack the C-terminal hemopexin-like domain present in the other MMPs, digest ECM components as gelatine and fibronectin. The membrane-type matrix metalloproteinases (MT-MMP), MMP-14, MMP-15, MMP-16, MMP-17, MMP-24 and MMP-25, have the ability to activate pro-MMP-2, and digest laminin, gelatine and fibronectin [76]. The remaining MMPs, MMP-12, MMP-19, MMP-20, MMP-21, MMP-23, MMP-27 and MMP-28, form a heterogeneous subgroup because they have a different amino acid sequence, domain organisation, or they do not have the same substrate specificity as the other MMPs, but in general they cleave elastine and aggrecan [79]. Most MMPs are secreted as inactive pro-proteins which are activated when cleaved by extracellular proteinases [80].

The TIMPs act as inhibitors by forming non-covalent 1:1 complexes with the MMPs, and has been shown to strongly promote liver fibrosis development, TIMP-1 is the main player in this process [81]. In addition to MMP inhibition, TIMPs have been shown to be multifunctional proteins that display growth factor-like activity and can inhibit angiogenesis [82].

Both normal and pathological tissue remodelling is regulated by the balance in expression of MMPs and TIMPs, and several pathological conditions result from an imbalance between them [83]. In normal tissue the MMPs and TIMPs are important for wound healing [84], embryotic development, collagen-turnover [85], endometrial menstrual breakdown, regulation of vascularization and the inflammatory response [86] to mention some. The over-expression of MMPs are often

associated with chronic inflammatory diseases, vascular diseases and tumor growth and metastases [87–89].

Table 1.1: **The MMPs** The matrix metalloproteinases are divided into subgroups based on their substrate specificity and the organization of their peptide domains. MMP; matrix metalloproteinases, MT-MMP; membrane-type matrix metalloproteinases, Col; collagen. Table modified from [79]

Subgroup	MMP	Name	Substrate
1. Collagenases	MMP-1	Collagenase-1	Col I, II, III, VII, VIII, X, gelatine
	MMP-8	Collagenase-2	Col I, II, III, VII, VIII, X, aggrecan, gelatine
	MMP-13	Collagenase-3	Col I, II, III, IV, IX, X, XIV, gelatine
2. Gelatinases	MMP-2	Gelatinase A	Gelatine, Col I, II, III, IV, VII, VIII, X
	MMP-9	Gelatinase B	Gelatine, Col IV, V
3. Stromelysisns	MMP-3	Stromelysin-1	Col II, IV, IX, X, XI, gelatine
	MMP-10	Stromelysin-2	Col IV, laminin, fibronectin, elastin
	MMP-11	Stromelysin-3	Col IV, laminin, fibronectin, aggrecan
4. Matrilysins	MMP-7	Matrilysin-1	Col IV, laminin, fibronectin, gelatine
	MMP-26	Matrilysin-2	Fibrogen, fibronectin, gelatine
5. MT-MMP	MMP-14	MT1-MMP	Gelatine, fibronectin, laminin
	MMP-15	MT2-MMP	Gelatine, fibronectin, laminin
	MMP-16	MT3-MMP	Gelatine, fibronectin, laminin
	MMP-17	MT4-MMP	Fibrogen, fibrin
	MMP-24	MT5-MMP	Gelatine, fibronectin, laminin
	MMP-25	MT6-MMP	Gelatine
6. Others	MMP-12	Macrophage metalloelastase	Elastin, fibronectin, Col IV
	MMP-19		Aggrecan, elastin, fibrillin, Col IV, gelatine
	MMP-20	Enamelysin	Aggrecan
	MMP-21	XMMP	Aggrecan
	MMP-23		Gelatine, casein, fibronectin
	MMP-27	CMMP	Unknown
	MMP-28	Epilysin	Unknown

1.5 Reversibility and resolution

Liver fibrosis is a dynamic process which is proven reversible. Resolution of fibrosis can be achieved by several mechanisms, both spontaneous and therapeutically [2, 90]. Spontaneous resolution of liver fibrosis can occur if the damaging agent is

removed or the underlying disease is treated [91]. Increased activity of the MMPs is the major mechanism of fibrosis resolution, through the decreased expression of TIMP-1. The interaction between partly degraded ECM and activated HSC induces apoptosis of activated HSC, thus terminating their production of pro-fibrotic products such as TIMP-1 [91, 92].

Finding a treatment for liver fibrosis has proven difficult. There are currently no standard treatment, and the only curative approach is liver transplantation [2, 93]. Several therapeutic approaches have proven effective in experimental models, such as removal of the causative agent, suppressing hepatic inflammation, inhibition of activation and proliferation of HSC, modulation of collagen synthesis and degradation, and specific targeting of anti-fibrotic therapy on the HSC [94]. Removing the causative agent has proven effective in humans [94, 95], but the efficiency and safety of the other treatments are not known and they may result in undesirable side effects such as liver impairment or cancer development [2, 94].

1.6 NaHS

Several compounds are used to reverse the fibrotic process in experimental models, one of these is sodium hydrogen sulfide (NaHS), which has been shown by several studies to attenuate fibrosis in rodent models [96, 97]. The active molecule is hydrogen sulfide (H_2S) which is shown to be endogenously generated in the body by the cystathionine γ-lyase (CSE)and cystathionine β-syntase (CBS) [98]. CSE and CBS are pyridoxal-5'-phosphate-dependent enzymes shown to be expressed in various tissues [99], their main substrate is L-cysteine, and their production of endogenous H_2S is shown to be involved in the pathogenesis of lung ischemia-reperfusion injury [100].

Administration of NaHS resulting in elevated levels of H_2S, has been shown to inhibit oxidative stress and proliferation of activated HSC. This induces cell cycle arrest and apoptosis of the activated HSC [101], thereby having a reverting effect on liver fibrosis [97, 102].

1.7 Fibrosis model organisms

To get a better understanding of the fibrosis mechanisms and development in the liver, several experimental models for liver fibrosis have been developed [103, 104].

The models differ in the way the fibrosis is induced in the animals. Chemically induced fibrosis often leads to hepatocyte death and necrosis [104]. Hepatotoxic agents such as CCl_4, thioacetamide (TAA), dimethylnitrosamine or alcohol are administered to experimental animals [104], leading to development of liver fibrosis within weeks after the start of treatment [105]. Another aspect of induction of fibrosis by chemical agents is the possibility to investigate the reversion of the fibrotic state by terminating the chemical treatment [106].

Induction of fibrosis with bile duct ligation (BDL) is a well studied experimental model, and the fibrotic response can be detected within weeks in the animals [107]. The fibrotic state resulting from BDL mimics the induction of fibrosis by extrahepatic biliary atresia and PSC, and is important for studying these diseases [104].

Immune-mediated fibrosis such as the chronic infection with hepatitis are often investigated by inducing liver fibrosis through the immune system with concanavalin A [104] which stimulates T-cells and induces an immune response [108].

Induction of spontaneous fibrosis in mice by the development of knock out (KO) or loss of function mice are used to study liver fibrosis [104]. One of the most prominent transgenic mouse models is the $Mdr2^{-/-}$ mouse used to study end stage liver fibrosis and the development of HCC in the liver as a result of fibrosis [109]. Most transgenic mouse models of fibrosis are characterised by impairment of regular functions in one or more liver cell types, leading to pathogenic ECM composition in the liver. The glycine N-methyltransferase (GNMT) KO mouse is a fibrosis model where a regulator of a catabolic pathway is disturbed, and the mouse develops a fatty liver which leads to fibrosis [110].

The difference between rodents and humans are a difficult barrier when developing model organisms for liver fibrosis. Several factors such as the difference between their immune systems, the time frame of fibrosis development and their metabolic rates makes it difficult to mimic the liver fibrosis development in humans. These factors also makes it difficult to transfer successful anti-fibrotic drug trials in rodent models, safely to anti-fibrotic drug trials in humans. The broad selection of fibrosis model organisms available is not sufficient to mimic the development of fibrosis in humans, and new model organisms are needed to be able to better understand fibrosis development and for drug trial with anti-fibrotic agents [103].

1.8 NCU-G1

Kidney predominant protein, NCU-G1, is a protein which is highly conserved among species. The mouse orthologue of the human C1orf85 [111] protein is approximately 43.8 kDa, has 404 amino acids, and is rich in proline [112, 113]. The *Ncug1* gene is localised on chromosome 3, and consist of 6 exons. NCU-G1 is highly expressed in liver, kidney and prostate and was initially described as be a nuclear protein functioning as a co-activator for peroxisome proliferator activated receptor α (PPAR-α), which is a major transcriptional regulator of lipid metabolism [114]. In the same study *NCU-G1* was also shown to be capable of functioning as a transcription-factor [112].

Later the protein was discovered to be a highly glycosylated integral lysosome membrane protein with a large luminal N-terminal domain, a transmembrane segment and a short cytoplasmic C-terminal tail (figure 1.3) [113]. The C-terminal tail contains a single tyrosine-based consensus lysosomal sorting motif at position 400 in the amino acid chain, and the protein has a molecular weight of approximately 75 kDa when fully glycosylated. The protein's cytoplasmic tail has some similarity to the cytoplasmic tail of lysosomal-associated membrane protein-1 (LAMP-1) and LAMP-2, but has no defined sequence homology to other proteins [113].

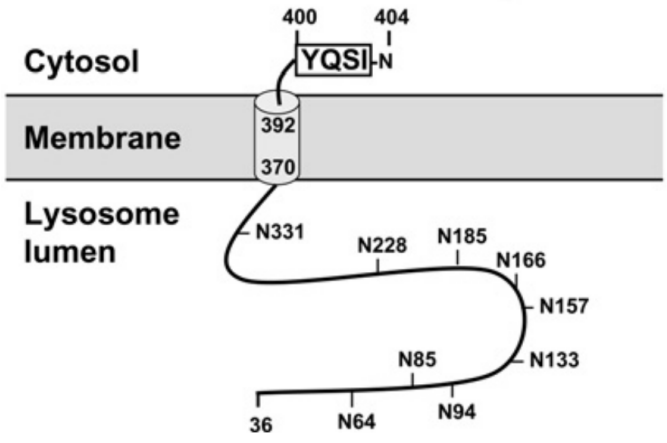

Figure 1.3: ***NCU-G1.*** The predicted topology of *NCU-G1* as a lysosomal transmembrane protein. The predicted glycosylation sites, transmembrane segment and potential tyrosine-based sorting signal are indicated. Figure modified from [113]

1.8.1 *NCU-G1*$^{gt/gt}$ mice

The *NCU-G1*$^{gt/gt}$ mice possess a gene-trap modification of the RIKEN cDNA 0610031J06 gene (*Ncug1* gene) (figure 1.4) and show no detectable expression of *Ncug1* [115]. The *NCU-G1*$^{gt/gt}$ mice are fertile and have a long life span. The only visible alteration from wild type (WT) mice is that the *NCU-G1*$^{gt/gt}$ mice have a severe liver fibrosis [115].

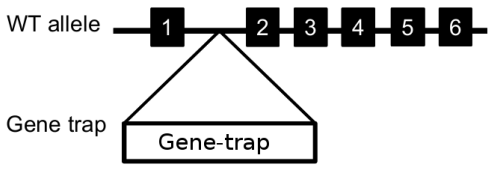

Figure 1.4: **The gene-trap.** A schematic representation of the gene-trap construct, inserted between exon 1 and 2 in the *Ncug1* gene. Figure modified from [115].

1.8.2 Lysosomal storage disease

Lysosomes are membrane-bound acidic organelles in eukaryotic cells that contain more than 50 different acid hydrolases, and are responsible for the catabolism of intracellular and extracellular macromolecules obtained by endocytosis and autophagy [116, 117]. Lysosomal storage diseases (LSD) are a class of metabolic disorders caused by mutations in proteins which are critical for the lysosomal function [118] which makes the cells unable to degrade the materials normally processed through the lysosomal pathway [119]. More than 50 LSD have been identified [120], and storage of undegradable substrates within lysosomes may lead to cellular dysfunction, chronic and progressing clinical syndromes, and can often result in dysfunction of the central nervous system (CNS) [120, 121]. The liver is often afflicted in LSD, and the degree of affliction depends on the disorder [122]. The specific organ affliction in LSD is influenced by tissue specific lysosomal enzyme content, substrate composition and rate of cell replacement [122, 123]. The CNS is especially sensitive to LSD since nerve cells do not undergo cell division and the lysosomal accumulation of undegraded substances is faster in long-lived post-mitotic and senescent cells [124].

Gaucher disease which is one of the most prevalent LSD and Niemann-Pick disease type C are among the LSD that lead to liver fibrosis [125,126]. Gaucher disease is caused by the deficiency of the enzyme glucocerebrosidase, and macrophages filled with the enzyme substrate glucosylceramide migrate to the liver, spleen, bone marrow and, in severe cases, the lungs, and induce fibrosis in these tissues [125, 127]. Niemann-Pick disease type C (NPC) comes from the loss of the function of the protein Niemann-Pick C1 or C2, which leads to the accumulation of free cholesterol and glycosphingolipids in the late endosomes and lysosomes. NPC can lead to neurodegeneration, hepatosplenomegaly, ataxia, seizures, and dystonia, and with the abnormal lipid accumulation in liver it is common for these patients to develop liver fibrosis [126, 128].

Lysosomes play an important role, by fusing with autophagosomes and degrading their content, in the autophagic pathway (figure 1.5) [129]. LSD impairs the fusion between autophagosomes and lysosomes, impairing the autophagic flux and the cells accumulate autophagic substances such as dysfunctional mitochondria and ubiquinated proteins [129]. The accumulation of autophagic substances has been shown to lead to impaired mitochondrial function which is a source of ROS, and this will eventually induce fibrosis [130].

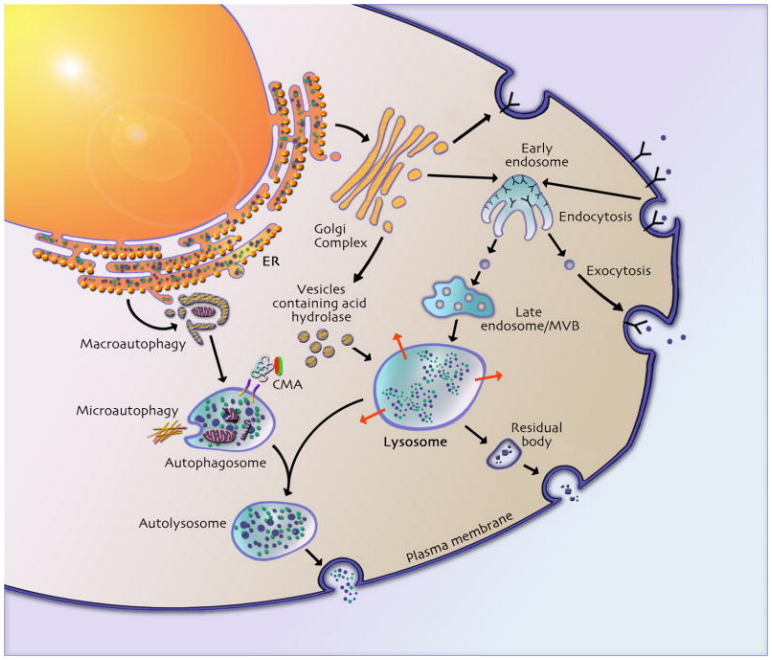

Figure 1.5: **The lysosomal pathway.** Schematic over the lysosomal pathway, and the interaction between lysosomes and autophagosomes to form autolysosomes. Figure modified from [118].

Chapter 2

Aim of the study

The *NCU-G1*$^{gt/gt}$ mice have been shown to develop liver fibrosis early in life [115], but mechanisms behind the fibrosis development are still unknown.

The aim of this study was to investigate the progression of liver fibrosis in the *NCU-G1*$^{gt/gt}$ mouse, the response to anti-fibrotic treatment with NaHS, in order to establish the *NCU-G1*$^{gt/gt}$ mouse as a model organism, and to explore possible causes for the development of liver fibrosis in the *NCU-G1*$^{gt/gt}$ mice.

The study can be divided into four sub-projects:

- Do the *NCU-G1*$^{gt/gt}$ mice have a metabolic disorder as a reaction to the lack of *Ncug1* expression, that is reflected in their weight gain and food consumption?
- How does the fibrosis progress in the *NCU-G1*$^{gt/gt}$ mice?
- Do the *NCU-G1*$^{gt/gt}$ mice respond to treatment with anti-fibrotic agents such as NaHS?
- Do the *NCU-G1*$^{gt/gt}$ mice have an impairment of the autophagic pathway which might be a result of a lysosomal storage disorder?

Chapter 3

Methods

3.1 Molecular biology techniques

3.1.1 Isolation of RNA from tissue

RNA was isolated from liver with RNeasy Plus Mini Kit from Qiagen and Fastprep-24 Lysing matrix tubes from MP. The kit integrates phenol/guanidine-based sample lysis and silica-membrane purification of total RNA, removes genomic DNA contamination with a gDNA Eliminator Solution without DNase digestion, and does not require a subsequent clean-up procedure to obtain good RNA purity and yield [131].

General procedure:

- β-mercapthoethanol (14.3M) ($10\mu l/ml$) was added to RLT Plus buffer (RNeasy Plus).
- RNAlater treated tissue (20mg) was transferred to a Lysing matrix tube with 1.4mm ceramic spheres containing RLT Plus buffer ($600\mu l$).
- The samples were homogenized in a FastPrep^{TM} FP 120, from Thermo Scientific, at level 4 for 40sec, repeating 4 to 5 times.
- The samples were placed regularly on ice to avoid overheating.
- The samples were then centrifuged at 15000xg for 3min at room temperature.

- The supernatant was transferred into a gDNA-eliminator-column, mounted on a 2ml tube.

- The tubes were centrifuged at 13000xg for 1min.

- 1 volume (600μl) of EtOH 50% was added to the flow through, mixed by repeated pipetting, and left for 5 min.

- 600μl of the sample was transferred to an RNeasy column mounted on a 2ml tube, and the lid was closed carefully.

- The tubes were centrifuged at 13000xg for 1min, the flow through was discarded and the rest of the sample transferred to the RNeasy column and the centrifugation was repeated.

- RW1 buffer (700μl) was added to the column, and the column was inverted a few times to wash the entire column with the RW1 buffer.

- The columns were centrifuged at 13000xg for 1min, and the flow-through was discarded.

- The columns were centrifuged again at 13000xg for 1min.

- RPE buffer (500μl) was added (4 volumes of 96-100% EtOH was added to the buffer before first time use), and the lid closed and the column inverted a few times to wash the entire column.

- The columns were centrifuged at 13000xg for 1min, and the flow-through discarded.

- RPE buffer (500μl) was added, the lid closed and the column inverted a few times to wash entire column.

- The columns were centrifuge at 13000xg for 1min, and the flow through discarded.

- The columns were transferred to new tubes (drying the outside of the columns with a paper-towel before placing them in the new tubes).

- The columns were centrifuged at 13000xg for 3min to remove any remains of EtOH.

- The columns were transferred to new 1.5ml tubes.
- RNAse-free H_2O ($50\mu l$) was added and the lids closed carefully.
- The tubes were centrifuged at 13000xg for 1min.
- The supernatant contained the isolated RNA.

3.1.2 Quantification of RNA using NanoDrop

All nucleotides absorb light at 260nm. When measuring the RNA concentration, the sample must be pure of DNA before measuring, to ensure that DNA will not contribute to the total absorbance. The Nanodrop gives values on 260/280nm and 260/230nm when measuring RNA concentration, to ensure that the sample is not contaminated with reagents or other cell components. The 260/280nm measurement gives an indication of the RNA-sample purity. A value much lower than 2.0 for RNA indicates contamination of protein, phenol or other substances that absorb light at approximately 280nm. A 260/230nm value significantly lower than 2.0 indicates that the sample contains contaminants that absorb light at 230nm such as carbohydrate, phenol or reagents used to isolate the nucleotides [132].

General procedure:

The RNA concentration was measured on a NanoDrop 2000 spectrophotometer, from Thermo Scientific, where $2\mu l$ of the sample was applied to the instrument and analysed.

3.1.3 cDNA synthesis

cDNA is synthesized from mRNA by reverse transcriptase (RT). RT is an enzyme able to use RNA as a template to synthesize DNA in a process called reverse transcription. This enzyme is used by retroviruses to be able to reproduce in their host organisms [133]. cDNA is further used as template in the amplification process (polymerase chain reaction (PCR)) that exponentially amplifies the cDNA.

Roche Transcriptor first strand cDNA syntesis kit was used [134]

General procedure:

- 2000ng mRNA was mixed with random hexamer primer ($2\mu l$) and RNAse-free water to total volume $13\mu l$.
- The samples were incubated at 65^0C for 10min, and transferred to ice.
- Master mix was prepared according to table 3.1.

Table 3.1: **Master mix for cDNA synthesis** The volumes indicate the master mix volume/sample:

5xRT-buffer	$4\mu l$
Anti.RNase	$0.5\mu l$
dNTP	$2\mu l$
RT-enzyme	$0.5\mu l$
Total volume	$7\mu l$

- The samples ($13\mu l$) were mixed with the the master mix ($7\mu l$), to a total volume of $20\mu l$.
- The samples were incubated in the PCR machine, using the temperature programme described in table 3.2.

Table 3.2: **The PCR programme used for cDNA synthesis:**

Step	Temperature(^{0}C)	Time(min)
1	25	10
2	50	60
3	85	5
4	4	∞

- The samples were diluted 1:2 with RNAse-free water after cDNA synthesis.

3.1.4 Quantitative real time-PCR

Quantitative real-time PCR (qRT-PCR) is a PCR reaction where the amplification of DNA is detected as the reaction progresses in real time. The amplification of template is detected by the binding of a fluorescent-dye that interacts with dsDNA [135]. The melting curve (Tm) indicates when 50% of the DNA is denatured, and the amount of product (cycle threshold (Ct)), can be measured by the fluorescent-light emitted from the fluorescent-dye interacting with the synthesized dsDNA [135]. The Ct value is the number of cycles that is required for the fluorescent signal to exceed the threshold (the background level), and is applied for measuring gene expression [89]. To be able to calculate the regulation of a gene, a housekeeping gene is always included to set the baseline regulation for the cells. The housekeeping genes are constitutive genes that are required for basal cellular functions, and are expressed at relatively constant levels during both pathological and non-pathological conditions [136, 137] .

The Roche LightCycler 480 DNA SYBR Green I Master kit was used for the qPCR.
The pre-primed plate provided was Hepatotoxicity PCR Array from Qiagen SABiosciences.

3.1.4.1 Hepatotoxicity PCR Array

General procedure:

- cDNA was added to the qRT-PCR master mix from the manufacturer, and the samples was aliquoted into the wells in the PCR array.
- The plate was processed on LightCycler® 480 from Roche, with PCR programme from the manufacturer.
- Data analysis of PCR data was performed with manufacturers software online.

3.1.4.2 qRT-PCR analyses of genes of interest

General procedure:

- Master mix was prepared for each gene, according to table 3.3.

Table 3.3: **Master mix for qRT-PCR** The volumes indicate the master mix volume/reaction:

Master mix 2X	$5\mu l$
Primer Fwd	$0.5\mu l$
Primer Rev	$0.5\mu l$
Super water	$3\mu l$
Total volume	$9\mu l$

- The master mix with primers ($9\mu l$) was transferred to each well, of the 96 well plate, together with cDNA ($1\mu l$). Gene expression analyses were conducted on 4 biological replicates and 3 technical replicates.
- The plates were processed with Roche SYBR-Green 96 well programme I on LightCycler® 480 from Roche.
- Tm and Ct values were measured, the Tm curves were evaluated to sort out invalid data, and the Ct values used for measurements of the gene expression.
- The results were standardised with the method described in [136], and presented as fold regulation, *NCU-G1*$^{gt/gt}$ vs WT.

3.1.5 Genotyping

Genotyping is a process where animals are separated according to their genetic make-up. The *NCU-G1*$^{gt/gt}$ mice can be separated from wild-type and heterozygous mice by two specific primer sets, *Ncug1* and the *gene-trap*. A PCR was performed with primers for *Ncug1* and the *gene-trap* (figure 3.1, table A. A.1), and the expected fragments identified on an agarose gel.

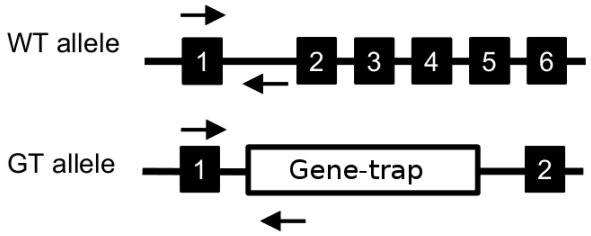

Figure 3.1: **Genotyping primer sites.** Schematic indication of the primer hybridization sites, shown with arrows. The WT allele transcribe the *Ncug1* gene fragment from the start of exon 1 to the star of exon 2 in the *Ncug1* gene which consist of 6 exons. The GT allele transcribe a gene fragment from the start of exon 1 to 1/3 of the *gene-trap* which is inserted between exon 1 and 2 in the *Ncug1* gene. Figure modified from [115]

General procedure:

- Genotyping lysis buffer (table A.B.12) was mixed with Proteinase K (Thermo Scientific) ($200\mu l/ml$) in a total volume of $350\mu l$ per ear-sample.
- Each ear sample was incubated in Proteinase K enriched lysis buffer ($350\mu l$).
- The samples were incubated at 55^0C with soft stirring for 3 hours.
- The samples were centrifuged at 17000xg for 10min at room temperature, and the supernatant transferred to a new tube.
- An equal amount isopropanol ($350\mu l$) was added to precipitate the samples.
- The samples were shaken horizontally for 5 min and left on the bench for 30 min.
- The samples were centrifuged at 14000xg for 30min at 4^0C.
- The supernatant was removed carefully.
- The pellets were washed in 96% EtOH (0.5ml).
- The samples were centrifuged at 14000xg for 10 min at 4^0C.
- The supernatant was removed, and the tubes dried upside down for 15 min.

- The tubes were turned the right way, and dried an additional for 30 min.
- 1mM Tris pH 8.0 ($30\mu l$) was added to dissolve isolated DNA.
- The DNA concentrations were measured using NanoDrop.
- A PCR with primers for *Ncug1* and *gene-trap* was performed, (200ng) sample (8μl) was mixed with master mix (48μl) according to table 3.4, and PCR steps 2-4 were repeated 30 times according to table 3.5.
- The DNA samples together with GeneRuler; 1 kb DNA standard (figure A. C.1) were separated with 80V on a 1% agarose gel, and visualised with ethidium-bromide (EtBr) under UV-light in a UVI-tec photo machine from Tamro med-lab.

Table 3.4: **Master mix for genotyping PCR** The volumes indicate the master mix volume/sample:

Buffer (10X)	$5\mu l$
Primer Fwd	$2\mu l$
Primer Rev	$2\mu l$
Super water	$31\mu l$
Dynazyme	$1\mu l$
dNTP (10mM)	$1\mu l$
Total volume	$48\mu l$

Table 3.5: **The PCR programme used for genotyping:**

Step	Temperature(^{0}C)	Time	Repetitions
1	94	5min	
2	94	30sec	step 2-4
3	59	30sec	were repeated
4	72	1min	30 times
5	72	5min	
6	4	∞	

3.1.6 Design of qRT-PCR primers

When designing primers it is important to take into consideration the quality of the primer such as the ability to anneal to itself and the gene, and the specificity of the primers. Primers should be between 18 bp and 30 bp long, a primer-length of 20 is optimal. An equal amount of purines and pyrimidines is an advantage, and the GC content of the primers should exceed 40% to ensure good binding of the primer to the template. The primers should not form hairpin loops or be complementary with itself (make homodimers) or the opposite primer (make heterodimers). The melting-point of the primers should be equal for both primers and not exceed room temperature for potential primer dimers. A product length between 100-200bp for the gene of interest is preferred, when the product is longer the enzymes in the PCR need more time to make the full complement strand, and the large product size influence the efficiency of the amplification process. The primers should not produce unspecific products, and only amplify the gene of interest during the qRT-PCR. If unspecific products are inevitable the product should exceed a length of 1000bp, this is to ensure that the product is not amplified because of the lack of time to amplify the long product [138].

General procedure:

- The primers were designed in the program Primer3 from the website http://simgene.com/Primer3. The program designs primers of suitable length and considers parameters as GC%, melting temperature and product length.
- The primers were checked for target gene with the Primer-BLAST on http://www.ncbi.nlm.nih.gov/tools/primer-blast/index.cgi?LINK_LOC=BlastHome.
- Self-dimerisation, hetero-dimerisation and hairpin loop structures were analyzed with OligoAnalyzer 3.1 on http://eu.idtdna.com/analyzer/applications/oligoanalyzer/
- Melting temperature was double checked with PrimerAnalyser on http://www.primerdigital.com/tools/PrimerAnalyser.html.
- The primers were ordered from DNA Technology (table A.A.2).

3.2 Protein techniques

3.2.1 Isolation of protein from tissue

Cell fractionation is a method used to separate different cell components. First the cells need to be lysed and the suspension homogenized. There are several ways to lyse tissue-cells, by sonication (sound waves), freezing the cells will destruct the cell organelles and the cells, enzyme digestion of the tissue-cell membrane or adding chemicals that break or distort the cell membrane. After the homogenization the sample is centrifuged to separate the different soluble and non soluble components in a suitable buffer.

General procedure:

- Mortar and other equipment were placed on dry ice to keep the samples frozen.
- The collected frozen liver (stored at -80^{0}C) was crushed to a fine powder in the mortar.
- Approximately 0.1g of the powder was weighed out in a centrifuge tube. The rest of the powder was stored or used for acid-hydrolysis.
- Lysis buffer (1ml) was added to each sample and the samples were vortexed and homogenized with a tissue homogenizer, from OMNI international, (2x15sec).
- The tissue homogenizer was washed with ethanol and MQ water (cooled) between each sample.
- The samples were kept on ice after homogenization.
- The samples were centrifuged for 25min, with 15000xg at 4^{0}C.
- Supernatant and pellet were separated and glycerol was added to the supernatant to a final concentration of 10%(v/v), before flash freezing in liquid N_2, and the samples were transferred to -80^{0}C.

3.2.2 Protein quantification with Bradford protein assay

The coomassie brilliant blue G-250 dye, used in the Bradford protein assay, shifts absorption wave-length from 465 nm to 595 nm when binding to protein, and

has different color-intensities with various concentrations of protein in the sample [139]. When a standard-curve with known concentrations is produced, the unknown concentration in the samples can be calculated.

General procedure:

- A standard-curve was made of bovine serum albumin, with the concentrations 0, 0.05, 0.1, 0.2, 0.3, 0.4 and $0.5 \mu g/ml$.
- The standards and samples ($10 \mu l$) were transferred to a 96 well reading plate in triplicates.
- Biorad protein assay dye was diluted 1:5 with MQ water and filtrated before use.
- The diluted Biorad protein assay ($200 \mu l$) was added to the samples and the standard-curve and left at room temperature for 5min.
- The absorption at 595 nm was measured using the Macelan programme in a Tecan sunrise plate reader.
- A standard-curve was made and the protein concentration calculated.

3.2.3 Hydroxyproline assay

Hydroxyproline is a hydroxylated form of the imino acid proline, which is performed by prolyl 4-hydroxylase (figure 3.2) [140]. Hydroxyproline is mainly present in the triple helix of collagen, as a stabiliser of the helix, and can in tissue hydrolysates, be used as a direct measure of the amount of collagen present in tissue. Hydroxyproline is obtained upon hydrolysis of collagen with strong acids, the levels measured represent all the types of collagen present in the sample without discriminating between the types of collagen [141].

QuickZymes hydroxyproline kit was used and the assay principle is shown in figure 3.3.

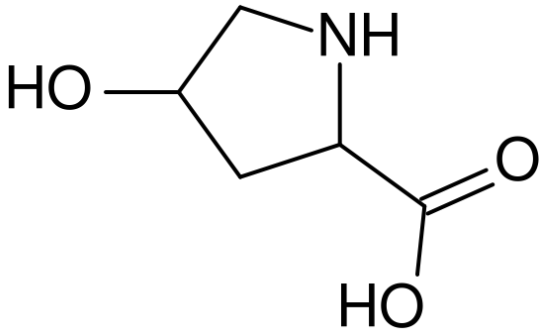

Figure 3.2: **The structure of hydroxyproline.** [142]

General procedure:

- Pulverized liver was hydrolyzed in 6M HCl (0.1g liver / 1ml HCl) by incubating the samples at 100^0C overnight.
- The hydrolyzed samples were vortexed, then centrifuged for 10min at 13000xg.
- The samples were diluted 1:2 with 4M HCl.
- The standard-curve was prepared from the stock solution to give a standard-curve with the concentrations 0, 12.5, 25, 50, 100, 200 and 300 μM.
- The standards and the samples ($35\mu l$) were transferred to a 96-well plate (2 technical replicas of the standards, 3 technical replicas of each sample, and 4 biological replicas).
- Assay buffer ($75\mu l$) was added to the standards and samples.
- The plate was covered with plastic and incubated at room temperature, for 20min, while shaken.
- Detection reagents A and B were mixed 2:3 in a total volume of $75\mu l$ per well, and the mix was added to the wells.
- The plate was covered with plastic and shaken to mix the reagents, then incubated for 1 hour at 60^0C.
- After incubation the plate was cooled on ice.
- The absorption at 570 nm was analyzed with the Macelan programme in a Tecan sunrise plate reader.

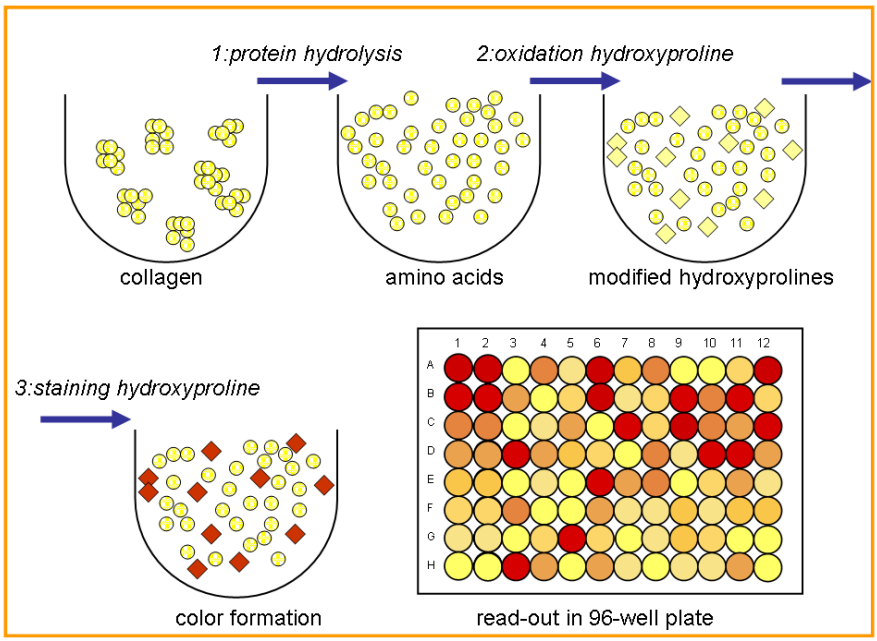

Figure 3.3: **Hydroxyproline assay principle.** Collagen is hydrolyzed with a strong acid. The hydroxyproline residues become oxidised, and stained. The hydroxyproline content in the samples are measured from their color intensity and calculated from a standard-curve. Figure modified form [141]

- The data was analyzed, and the hydroxyproline content in liver calculated, and presented as μg hydroxyproline/g wet liver weight.

3.2.4 SDS-PAGE

Sodium dodecyl sulphate polyacrylamide gel electrophoresis (SDS-PAGE) is a method to separate proteins according to their size. SDS is an anionic detergent that denatures proteins by forming complexes of 1 SDS molecule per 2 amino-acids in the protein, giving the proteins a negative charge. SDS breaks the non-covalent bonds in native proteins and the samples are boiled to denature the protein completely. The proteins can be separated according to their size on a gel, since binding of SDS makes the protein length proportional to its molecular weight. Small proteins will migrate faster in the gel than big proteins, and the speed of protein migration is regulated by the concentration of polyacrylamide in the gel [143].

The gels used are NuPAGE® Novex® 10% Bis-Tris Gels, 1.0 mm, 12 well from Life Tech.

General procedure:

- The protein samples were diluted to $100\mu g/ml$ with MQ water.
- The samples were mixed with sample buffer B.2) to give a total volume of $25\mu l$.
- The samples were incubated at 96^0C for 10min, and centrifuged.
- The samples ($20\mu l$) and the protein standard PageRuler; Prestained protein ladder (figure A. C.2)($5\mu l$) were loaded onto the SDS-gel.
- The electrophoresis buffer used was 1xMOPS SDS Running buffer provided by the manufacturer.
- The proteins were separated at 200V (150A/gel) for 45 - 60 min.

3.2.5 Western blotting

Western blotting is a method used to detect the presence of a specific protein in the sample with the help of antibody labeling. The proteins are first separated based on their size by SDS-PAGE, before they are transferred to a membrane by electrotransffering. The proteins are labeled with primary antibodies after the unspecific binding sites are blocked. A secondary antibody which recognizes the Fc region of the primary antibody is added. The secondary antibody usually possesses a conjugated reporter enzyme such as horse radish peroxidase (HRP). A specific substrate for this enzyme is then added to produce a detectable signal. HRP and peroxide catalyzed oxidation of the Lumigen PS-3 Acridan substrate will generate acridinium ester intermediates. This intermediate react with peroxide under slight alkaline conditions, and produce a chemiluminescence that can be detected by a photo machine [144, 145]. After use the membrane can be stripped to remove the attached antibodies by changing the pH, thus altering the affinity of the antibodies for the proteins on the membrane. After stripping the membrane is ready for treatment with new antibodies [146].

General procedure:

3.2.5.1 Blotting

The membrane used was a polyvinylidene difluoride (PVDF) membrane from Bio-Rad.

- The SDS-gel was released from the gel cassette, and soaked in cold blotting buffer (table A.B.3).
- Two fiber-pillows and four sheets of Watman-filter were soaked in blotting buffer.
- The blotting membrane was first soaked in methanol and then transferred to blotting buffer.
- The blotting cassette was stacked in the order, bottom up; black part of blotting cassette, fiber pillow, 2x Watman-filter, SDS-gel, membrane, 2x Watman-filter, fiber pillow and the white part of the blotting cassette on top (figure 3.4).

Figure 3.4: **Western blotting cassette.** The blotting cassette is stacked in the order from cathode to anode; black part of blotting cassette, fiber pillow, 2x Watman-filter, SDS-gel, membrane, 2x Watman-filter, fiber pillow, white part of blotting cassette.

- The blot was placed in a blotting chamber, with the black part of the blotting cassette against the cathode and the white part against the anode.

- A magnet stirrer and a cooling element was placed in the chamber, and the chamber was filled with blotting buffer.

- The proteins were transferred from the gel to the membrane at 20V overnight at 4^0C.

3.2.5.2 Blocking

- Skimmed-milk-powder (2.5g) (Sigma) per 50ml 1xTBST (table A.B.5) was mixed, filtrated and used as blocking buffer.

- The blotting membrane was removed from the blotting cassette.

- The membrane was blocked with the skimmed-milk-powder enriched TBST for 1 hour with gentle shaking.

3.2.5.3 Antibody

- The primary antibody (table A.A.4) was diluted in skimmed-milk-powder enriched TBST.

- The blocking solution was replaced with the primary antibody solution.

- The membrane was incubated with mild shaking for 2 hours at room temperature.

- The primary antibody solution was removed.

- The membrane was washed in TBST buffer, first for 3x5min, and then 3x15min, with vigorous shaking.

- The secondary antibody (table A.A.4) was diluted in skimmed-milk-powder enriched TBST.

- The TBST buffer was replaced with the secondary antibody solution and incubated with mild shaking for 1 hour at room temperature.

- After 1 hour the secondary antibody solution was removed.

- The membrane was washed in TBST buffer, for 3x5min and 2x15min, with vigorous shaking.

- Finally the membrane was washed in TBS buffer, for 15 min, with vigorous shaking, and was ready to be visualized.

3.2.5.4 Visualizing

The visualizing kit Amershan-ECL Plus Western Blotting Detection Reagents was used.

- Kit solution A was mixed in an equal volume of kit solution B. The reagents are light sensitive and the tube must be covered in silver foil to protect the reagents.
- The mix was vortexed before use.
- The membrane was transferred to a glass plate with the protein side up.
- Visualizing solution was dripped on top of the membrane, covering it with the solution.
- The solution was left to work for about 1 min.
- Excess visualizing solution was removed, and the membrane was visualized on a Kodak Image station 4000R Pro.
- Pictures were taken with a ECL camera to visualise the luminesence light from the HRP reaction. Pictures was also taken in white light to visualise the standard.

3.2.5.5 Stripping

- The membrane was washed in MQ water for 30 sec with shaking.
- The membrane was incubated in 0.2M NaOH for 5 min at room temperature.
- The membrane was washed in MQ water for 30 sec with shaking.
- The membrane was transferred to TBS buffer, and this makes it ready for re-staining.

3.2.6 Gelatine zymography

The gelatinases, MMP-9 (92 kDa) and MMP-2 (72 kDa), can be detected by zymography with gelatine [79, 147]. Also MMP-1, MMP-8 and MMP-13 can be detected by this method [79]. The native proteins are separated according to their size on a gel containing gelatine, and the MMPs are allowed time to digest the gelatine after electrophoresis. The gelaine in the gel is stained and the site of the active gelatinases are visualised as clear bands on the gel were the gelatine has been digested.

The gels used were Novex® 10% Zymogram (Gelatin) Gel 1.0 mm, 12 Well from Life Tech.

General procedure:

- Protein samples were diluted to $0.5\mu g/\mu l$ with MQ water in a total volume of $11\mu l$.
- One part Sample buffer (table A.B.6) was added to one part sample and incubated for 10 min at room temperature.
- Samples ($10\mu l$) and standard PageRuler; Prestained protein standard ($5\mu l$) (figure A. C.2) were loaded on the Zymography gel.
- The proteins were separated at 125V (100A/gel) for 90-100min.
- After protein separation, the gel was transferred to 100ml renaturing buffer (table A.B.8) and incubated for 30min at room temperature.
- After removal of the renaturing buffer, the gel was incubated in 100ml developing buffer (table A.B.11) for 30min with gentle shaking.
- The developing buffer was replaced with new developing buffer and the gel incubated at 37^0C overnight.
- After the overnight incubation the developing buffer was removed, and the gel was stained with Simply Blue Coomassie safe stain from Invitrogen for 1 hour with vigorous shaking.

- The Simply Blue Coomassie safe stain was removed and the gel washed in MQ water for 30 min with mild shaking.

- The water was changed and the gel was left to destain with shaking until the bands became visible.

- Pictures were taken of the gel with a Canon EOS 550D camera.

3.3 Work with mice

All animal experiments were conducted according to national laws and regulations.

3.3.1 Measuring the weight and food consumption of mice

General procedure:
Animal weight development and food consumption were monitored once every 7 days. Food efficiency (change in weight (g)/food consumed (kcal) per week) was calculated.

The food provided was Rat and Mouse No.1 Maintenance Pelleted (SDS) which has a gross energy of 3,52 kcal/g food [148].

Food efficiency (change in weight (g)/food consumed (kcal) per week) = Average weight gain (g) / (calories per g food (kcal) * Average food consumed (g))

3.3.2 Termination of mice and collection of organs

General procedure:

- The mice were sedated with an anaesthetic Hypnorm-Dormicum.

  - MIDAZOLAM (Dormicum)and FLUANISON (Hypnorm) were both diluted 1:2 with water.

  - The diluted Hypnorm and Dormicum was mixed 1:1.

  - 0.005-0.0075 ml/g animal was administered.

  - Duration of anesthesia was 30 - 60 min.

- Fur and skin were removed to expose the rib cage and the saphenous vein.
- Blood was collected from the saphenous vein by making an incision in the vein, and the blood was collected with a pasteur pipette by capillary forces.
- In order to extract more blood, a needle mounted on a syringe was inserted directly in the heart of the mouse, just to the right of the sternum, between the 4 and 5 rib counted from below (figure 3.5). This procedure terminated the animal.

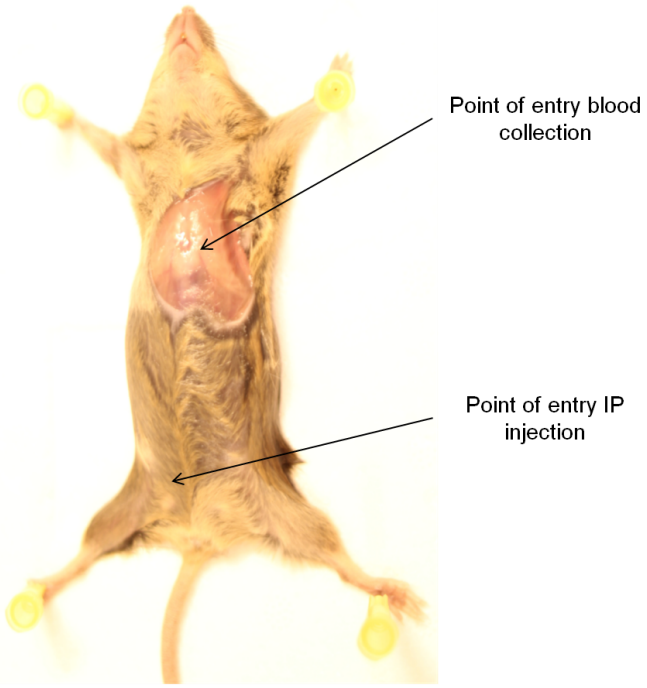

Figure 3.5: **Points of entry for blood collection and intraperitoneal injection.** The entry points for collection of blood during terminal procedures, and point of entry when administrating liquid substrates with intraperitoneal injection, on mice.

- The abdomen of the dead mouse was opened to expose the organs of interest; liver, kidney, spleen, heart, brain and skeletal muscle were collected. The livers was used further in this study.
- The liver and spleen were weighed and photographed.
- The data was analyzed, and the organ size, presented as % of body weight, was compared between the *NCU-G1*$^{gt/gt}$ and WT.

- Samples were collected in RNAlater (Ambion) to isolate RNA, and the remaining tissue was flash frozen in liquid N_2 and transferred to -80^{0}C for later use.

3.3.3 Intraperitoneal (IP) administration of NaHS

IP injection is an efficient method to administer substances to mice. The mice have to be properly restrained during the procedure to avoid damage to their internal organs. The needle filled with the NaHS solution, is inserted into the abdomen just beside the right leg of the mice, and the substance administered. The recommended needle size for mice is 25-27 gauge [101].

General procedure:

- NaHS was dissolved to $60\mu g/ml$ in sterile filtered PBS buffer.
- The mice were administered a dosage of $0.6\mu g/g$ body weight every other day for 30 days with IP injection (figure 3.5).
- The mice were terminated, and the livers were collected for later analyses such as qRT-PCR, hydroxyproline measurements and gelatine zymography.

3.3.4 Induction of autophagy

General procedure:

- The mice were starved for 24 hours, then allowed to feed for 1 hour for synchronization.
- After feeding the mice were starved for 24 hours, and the livers were collected.

3.4 Statistics

Double sided T-test with anticipated similar variance (Excel 2007) was performed for the weight, hydroxyproline and qRT-PCR data. A P-value below 0.05 was considered significant.

Chapter 4

Results

4.1 Genotyping

To confirm the genotype of the mice after a new mating the presence of the *gene-trap* in the *Ncug1* gene were investigated. DNA was extracted from mice ear samples and genotyping was performed (Ch.3.1.5) with primers for the *gene-trap* and *Ncug1*. A representative figure for the different genotypes is shown in figure 4.1.

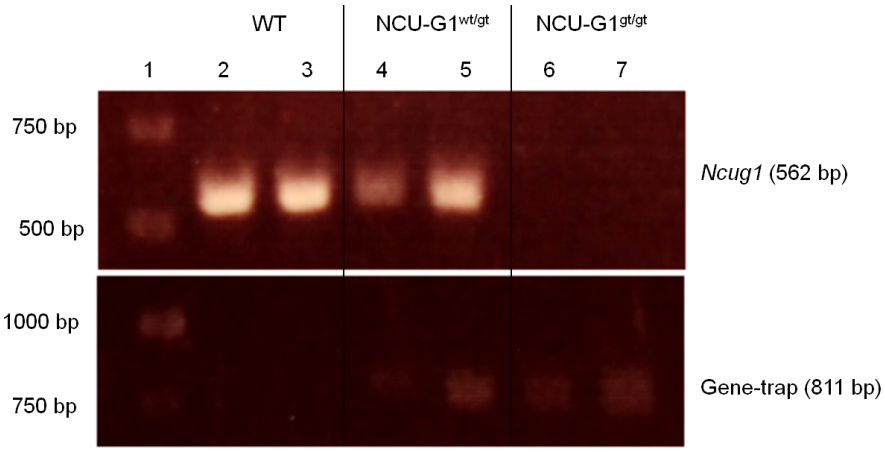

Figure 4.1: **Representative figure for the genotypes.** DNA was extracted from ear samples of mice, and polymerase chain reaction with primers for *Ncug1* and *gene-trap* was performed. The WT mice (lane 2 and 3) gives the *Ncug1* PCR fragment (562bp) and not the *gene-trap* PCR fragment (811bp). The heterozygous *NCU-G1*$^{wt/gt}$ mice (lane 4 and 5) gives both the *Ncug1* and the *gene-trap* PCR fragment. The *NCU-G1*$^{gt/gt}$ mice (lane 6 and 7) gives only the *gene-trap* fragment.

The figure 4.1 shows that a WT gives only the *Ncug1* PCR fragment (562bp)(lane 2 and 3). The heterozygous *NCU-G1*$^{wt/gt}$ mice gives both the *Ncug1* PCR fragmet (562bp) and the *gene-trap* PCR fragment (811bp) (lane 4 and 5). The homozygous *NCU-G1*$^{gt/gt}$ mice only give the gene-trap PCR fragment (811bp) (lane 6 and 7). The lack of *Ncug1* is proof that the gene-trap is inserted on both alleles, and theoretically *Ncug1* cannot be transcribed.

4.2 Weight study

The mice and food were weighed every 7 days(Ch. 3.3.1), and the weight gain and food consumption were monitored.

4.2.1 Individual weight development depends on number of cage habitants

The difference in weight gain is shown for cages with different numbers of inhabitants for males and females for both WT and *NCU-G1*$^{gt/gt}$ mice (figure 4.2). The data was pooled, with cages with 4 or 5 inhabitants shown against cages with 1, 2 or 3 inhabitants.

All the individuals had a rapid weight gain at an early age, measured from approximately 21 days of age, and after the mice reached approximately the age of 70 days their weight gain was less rapid. The male animals had approximately the same weight gain development in all cages at an early age, but the measured values for the cages with 1 to 3 inhabitants were spread when the mice grew older. The females in cages with 1 to 3 inhabitants had a tendency to gain weight faster early in their lifespan, and the data in these cages were not uniform. The weight gain values in the cages with fewer mice were spread for both male and female, *NCU-G1*$^{gt/gt}$ mice an WT mice, and could not be used for further studies.

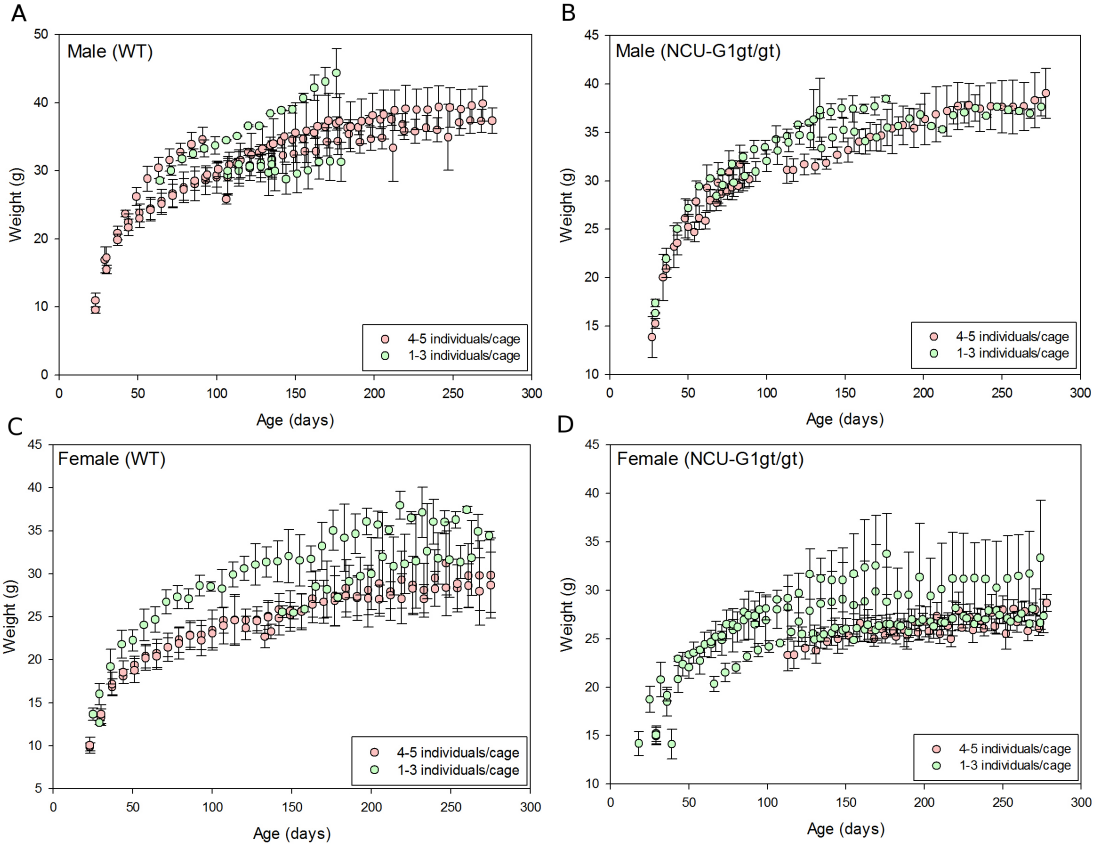

Figure 4.2: **Weight gain comparison based on cage inhabitants.** Mice weight development was monitored every 7 days, and the average weight per cage was calculated. The weight of mice in cages with 1 to 3 inhabitants were compared with cages with 4 to 5 inhabitants, based on their age for **(A)** male WT mice (1-3 inhabitants (n=10), 4-5 inhabitants (n=27)), **(B)** male *NCU-G1*$^{gt/gt}$ mice (1-3 inhabitants (n=10), 4-5 inhabitants (n=17)) **(C)** female WT mice (1-3 inhabitants (n=8), 4-5 inhabitants (n=12)) **(D)** female *NCU-G1*$^{gt/gt}$ mice (1-3 inhabitants (n=13), 4-5 inhabitants (n=13)).

4.2.2 Difference in weight between WT and *NCU-G1*$^{gt/gt}$ mice

Only individuals and food from cages with 4 or 5 inhabitants were used to monitor the difference in weight gain and food efficiency between WT and *NCU-G1*$^{gt/gt}$ mice (figure 4.3).

Both males and females had a rapid weight gain early in their life. After the mice reached approximately the age of 70 days the weight gain was less rapid. Both the males and females had a high food efficiency early in their life, and at

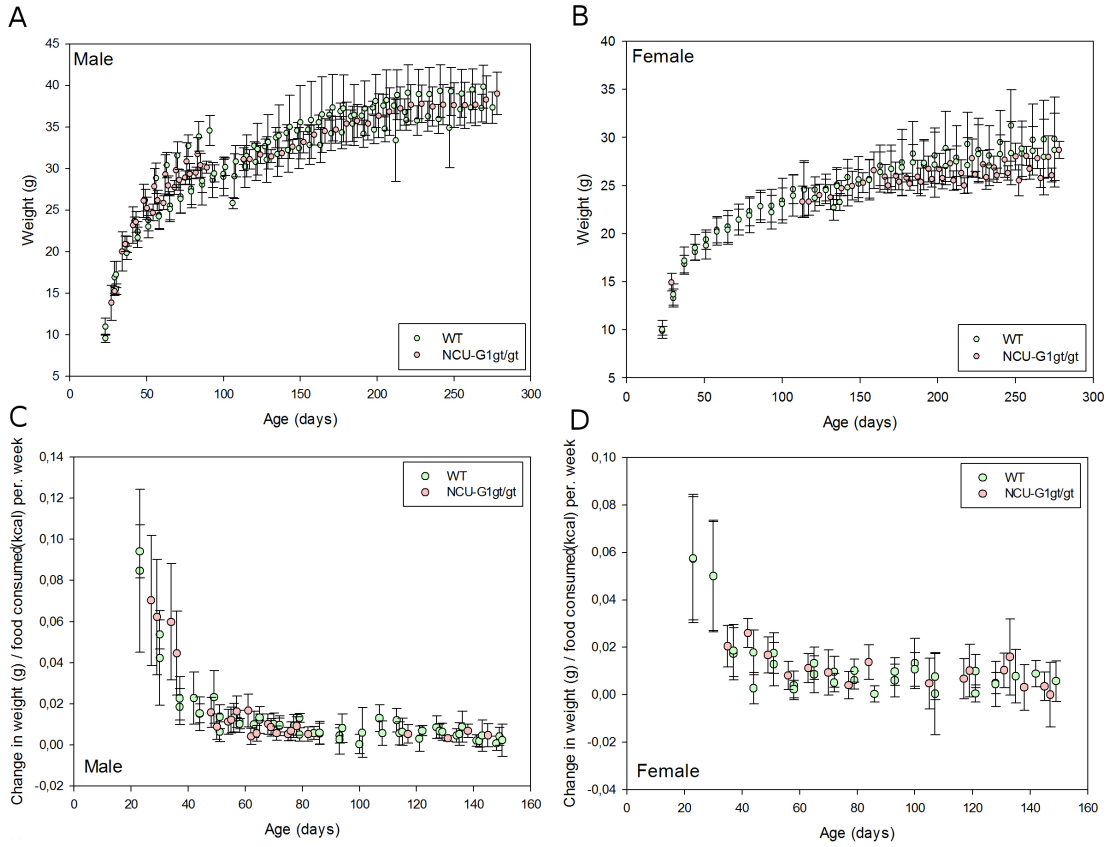

Figure 4.3: **Weight gain and food efficiency comparison between *NCU-G1$^{gt/gt}$* and WT mice.** weight gain and food consumption was monitored every 7 days, and the average weight and food efficiency per cage were calculated. The weight gain of WT mice was compared with *NCU-G1$^{gt/gt}$* mice, based on their age for **(A)** male mice(WT (n=27), *NCU-G1$^{gt/gt}$* (n=17)), **(B)** female mice (WT (n=12), *NCU-G1$^{gt/gt}$*(n=13)). The food efficiency in WT mice was compared to the food efficiency in *NCU-G1$^{gt/gt}$* mice, and given as change in weight (g)/food consumed (kcal) per week based on their age for **(C)** male mice(WT (n=27), *NCU-G1$^{gt/gt}$* (n=17)), **(D)** female mice (WT (n=12), *NCU-G1$^{gt/gt}$*(n=13)).

approximately the age of 50 days the food efficiency levels out and stabilizes. The data for weight gain and food consumption of the WT and *NCU-G1$^{gt/gt}$* mice overlap for both males and females, and there were no differences between the groups.

4.3 Progression of liver damage

4.3.1 Visible changes in liver appearance

Extracted mouse livers and spleen (Ch. 3.3.2) were examined and weighted before they were divided into samples. WT livers displayed no differences in shape or colour with age (figure 4.5). The *NCU-G1$^{gt/gt}$* livers started to visibly differ from the WT livers already at 3 weeks of age. These livers displayed small spots of discoloration that became more visible when the mice reached 1 month of age. When the mice reached 2 months of age the spots had become bigger and seemed to have fused together, and the shape of the livers was dented and not smooth like the WT livers. At the age of 3.5 months and at later time-points, age 4.5, 6, 7.5 and 9 months, the livers had lost their original shape completely, and the discoloration was prominent, as seen from the representative pictures in figure 4.5. There is a tendency to an enlargement of the liver in the *NCU-G1$^{gt/gt}$* mice (figure 4.4A). The spleens were compared between the *NCU-G1$^{gt/gt}$* and WT mice which displayed an enlargement of the spleens in the *NCU-G1$^{gt/gt}$* mice(figure 4.5). There is a significant enlargement of the spleens of *NCU-G1$^{gt/gt}$* mice at the ages 1, 2, 3.5, 4.5, 6 and 7.5 months (figure 4.4B).

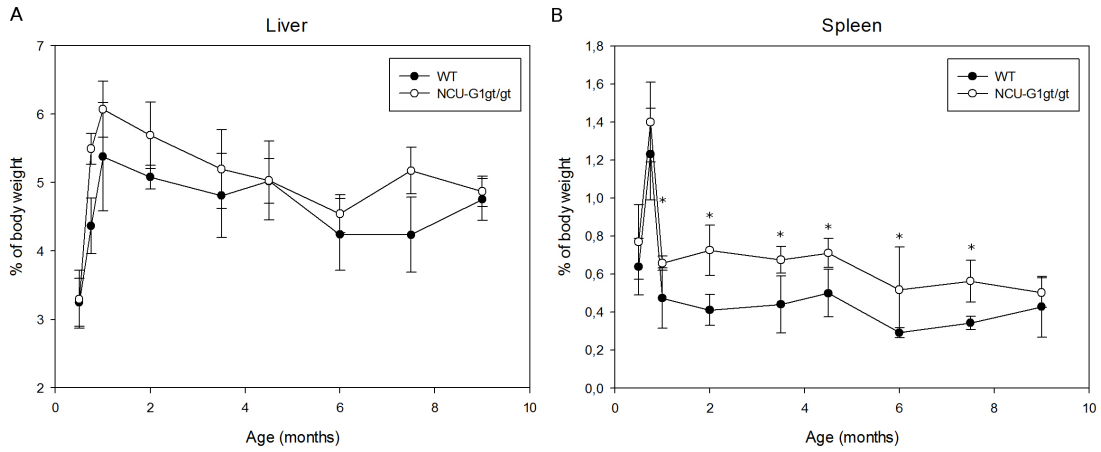

Figure 4.4: **Enlargement of liver and spleen in *NCU-G1$^{gt/gt}$* mice.** Livers and spleens from WT and *NCU-G1$^{gt/gt}$* mice was weighted, and the % of the bodyweight compared for **(A)** livers and **(B)** spleens. Stars indicate statistical significance (*p $\leq$ 0.05).

Figure 4.5: **Visible progression of liver damage in *NCU-G1*$^{gt/gt}$ and WT mice.**

Figure 4.5: *NCU-G1*$^{gt/gt}$ and WT mice were terminated at different ages and the livers collected. The visible development of the fibrosis in the *NCU-G1*$^{gt/gt}$ mice, and the lack of this development in WT mice, could be detected by investigating the color change and structure of the livers at the different time-points. The spleen was investigated for visible enlargement in the *NCU-G1*$^{gt/gt}$ mice. The pictures are representative for each time-point. The bar in the spleen pictures show 1 cm between each vertical line.

4.3.2 Liver hydroxyproline levels

Extracted livers (Ch. 3.3.2) were pulverized (Ch. 3.2.1), hydrolyzed in 6M HCl, and the hydroxyproline levels were measured (Ch. 3.2.3). Figure 4.6 shows the levels of hydroxyproline in WT and *NCU-G1*$^{gt/gt}$ liver from the age of 2 weeks until the age of 9 months.

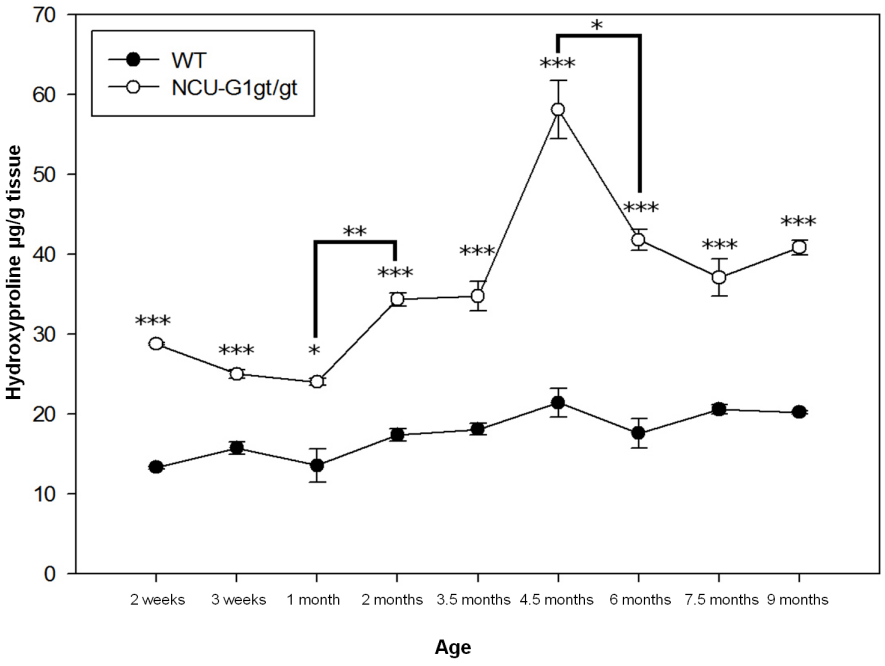

Figure 4.6: **The hyrdoxyproline content in *NCU-G1*$^{gt/gt}$ and WT liver.** Liver tissue from *NCU-G1*$^{gt/gt}$ and WT mice at different ages were pulverized, and the liver powder were hydrolysed in strong acid. QuickZymes hydroxyproline kit was used, and the hydroxyproline levels were measured, and presented as μg hydroxuproline/g wet tissue (n=4). Stars indicate statistical significance (*p $\leq$ 0.05, **p $\leq$ 0.05, ***p $\leq$ 0.05).

The hydroxyproline content in the WT mice had a small increase until it reached 4.5 months, where the hydroxyproline content were 21.39 μg hydroxyproline/g wet tissue, and then stabilized. The development of hydroxyproline content in the *NCU-G1*$^{gt/gt}$ mice liver increased until the mice reached 4.5 months of age, where the hydroxyproline content were 58.06 μg hydroxyproline/g wet tissue, and then decreased (figure 4.6). There were significant differences in hydroxyproline levels between the *NCU-G1*$^{gt/gt}$ and WT mice at all ages. There was a significant increase in hydroxyproline level in the *NCU-G1*$^{gt/gt}$ mice livers between the ages 1 month and 2 months, and a significant decrease in hydroxyproline level in the *NCU-G1*$^{gt/gt}$ mice livers between the ages 4.5 months and 6 months.

4.3.3 qRT-PCR

RNA was isolated from RNAlater preserved liver samples (Ch. 3.3.2, 3.1.1). The RNA concentrations were measured (Ch. 3.1.2), and cDNA were synthesized (Ch. 3.1.3) and used to analyze gene expression with qRT-PCR (Ch. 3.1.4).

4.3.3.1 Hepatotoxicity PCR Array

RNA from 3.5 months old mice were analyzed on a 96 well plate SABiociences Qiagen, readily primed for genes known to be involved in different aspects of the cellular response to hepatotoxicity (Ch. 3.1.4). Table 4.1 shows changes in gene expression for 3.5 months old *NCU-G1*$^{gt/gt}$ mice. Genes displaying more than 1.5 fold expression difference between *NCU-G1*$^{gt/gt}$ and WT mice are presented in this table.

The regulation of the hepatotoxcity cellular response genes indicate that the liver cells of the *NCU-G1*$^{gt/gt}$ mice were experiencing hepatotoxic conditions.

The most dramatic difference in the *NCU-G1*$^{gt/gt}$ mice relative to the WT was a 22.53 fold up-regulation of the S100 Calcium Binding Protein A8 (S100A8). This gene encodes a calcium- and zinc-binding protein which is found in high concentrations at local sites of inflammation, among them cystic fibrosis, and plays an important role in the immune response [149].

Table 4.1: **qRT-PCR data of the pre-primed plates:** 3.5 months old WT and *NCU-G1*$^{gt/gt}$ livers were investigated on a pre-primed plate (Qiagen SABiociences), and the fold regulation calculated. Only genes displaying more than 1.5 fold difference in expression between *NCU-G1*$^{gt/gt}$ and WT are included (n=3).

Symbol	Name	Fold Regulation
S100a8	S100 calcium binding protein A8	22.5
Col4a1	collagen, type IV, alpha 1	4.0
Thrsp	thyroid hormone responsive	3.0
Hmox1	heme oxygenase (decycling) 1	2.6
Icam1	intercellular adhesion molecule 1	2.2
Btg2	BTG Family, Member 2	2.2
Fasn	fatty acid synthase	2.2
Osmr	oncostatin M receptor	2.1
Osta	solute carrier family 51, alpha subunit	1.9
Cd36	CD36 molecule (thrombospondin receptor)	1.9
Hao2	hydroxyacid oxidase 2 (long chain)	1.8
Tagln	transgelin	1.8
Tmem2	transmembrane protein 2	1.7
Casp3	caspase 3, apoptosis-related cysteine peptidase	1.7
Fxc1	translocase of inner mitochondrial membrane 10 homolog B (yeast)	1.7
Cd68	CD68 antigen	1.6
Map3k6	mitogen-activated protein kinase kinase kinase 6	1.6
Scd1	stearoyl-CoA desaturase 5	1.6
Lpl	lipoprotein lipase	1.5
Cdkn1a	cyclin-dependent kinase inhibitor 1A	1.5
Hpn	hepsin	-1.5
Car3	Carbonic Anhydrase III	-1.5
Gclc	glutamate-cysteine ligase, catalytic subunit	-1.5
Fam158a	ER membrane protein complex subunit 9	-1.6
Igfals	insulin-like growth factor binding protein, acid labile subunit	-1.6
Abcc3	ATP-Binding Cassette, Sub-Family C (CFTR/MRP), Member 3	-1.7
Txnrd1	thioredoxin reductase 1	-1.7
Dnajb11	DnaJ (Hsp40) homolog, subfamily B, member 11	-1.7
Avpr1a	Arginine Vasopressin Receptor 1A	-1.8
BC031353	Family With Sequence Similarity 214, Member A	-1.9
Mbl2	mannose-binding lectin (protein C) 2, soluble	-1.9
Wipi1	WD repeat domain, phosphoinositide interacting 1	-1.9
Fabp1	fatty acid binding protein 1, liver	-2.0
Mlxipl	MLX interacting protein-like	-2.0
Bhmt	betaine–homocysteine S-methyltransferase	-2.2
Fmo1	flavin containing monooxygenase 1	-2.3
Lgr5	leucine-rich repeat containing G protein-coupled receptor 5	-2.7

4.3.3.2 qRT-PCR analyses of genes of interest

The genes of interest *MMP-2*, *MMP-9*, *TIMP1*, *S100A8*, *TGF-β1*, *α-smooth muscle actin (α-SMA)* and *Collagen type I α 1 (Col1α1)* were analysed by qRT-PCR, for ages between 1 and 9 months, for both WT and *NCU-G1*$^{gt/gt}$ mice (Ch. 3.1.4). The relative gene expression was normalized to the housekeeping gene eukaryotic translation elongation factor 2, and the data were analyzed to find the difference in gene expression (Ch. 3.4). Figure 4.7 shows the relative expression of the genes between *NCU-G1*$^{gt/gt}$ and WT mice at different age points.

All the genes of interest were expressed differently in the *NCU-G1*$^{gt/gt}$ relative to the WT mice. The expression of *MMP-2* increased until the mice reached 3.5 months of age where the gene was up-regulated 3.4 folds, after 3.5 months the expression decreased followed by a small increase at the age of 7.5 months (figure 4.7A).There were significant up-regulations of this gene at the ages 1, 3.5, 4.5 and 7.5 months relative to WT.

MMP-9 expression in *NCU-G1*$^{gt/gt}$ liver was significantly up-regulated at all ages except at ages 1 and 9 months relative to WT. The expression difference was highest at 3.5 months of age with a fold up-regulation of 12.7 in *NCU-G1*$^{gt/gt}$ liver (figure 4.7B).

One of the inhibitors of the MMPs, *TIMP-1* (figure 4.7C) was significantly up-regulated at all ages except at 9 months, and the highest expression was at age 4.5 months where it is 8.2 folds up-regulated in *NCU-G1*$^{gt/gt}$ liver relative to the WT.

S100A8 was shown to be the most up-regulated gene on the pre-primed plates (table 4.1). This was verified using qRT-PCR, where this gene was up-regulated significantly in *NCU-G1*$^{gt/gt}$ liver at all ages, and peaked with 416.3 fold up-regulation at the age of 4.5 months(figure 4.7D).

The known fibrotic markers *TGF-β1*, *α-SMA* and C*ol1α1* all show the same progression as the hydroxyproline data (figure 4.6). The expression of *TGF-β1* (figure 4.7E) and *α-SMA* (figure 4.7F) peaked at 3.5 months of age with an up-regulation of 3.3 and 3.5 folds, respectively, while *Col1α1* (figure 4.7G) has a peak at 4.5 months where it is 6.8 folds up-regulated relative to the WT. *TGF-β1* is significantly up-regulated at all ages except at 9 months, *α-SMA* was significantly up-regulated from the age of 3.5 months and older, and *Col1α1* was up-regulated significantly at 1, 3.5, 4.5 and 7.5 months of age.

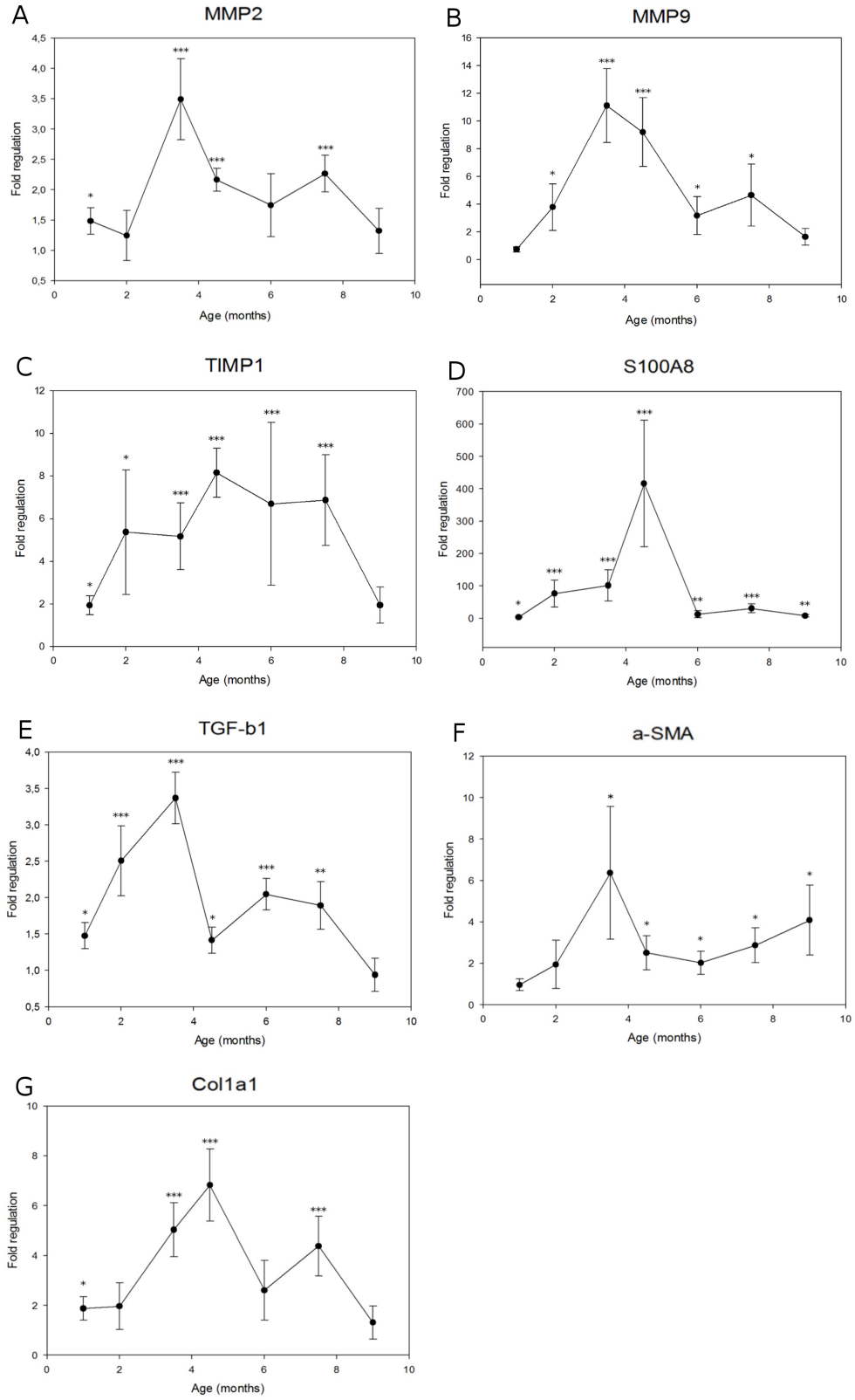

Figure 4.7: **Gene expression analysis of *NCU-G1*$^{gt/gt}$ and WT mice liver.** Difference in gene expression of selected genes involved in liver fibrosis were investigated with quantitative real-time polymerases chain reaction.

Figure 4.7: Difference in expression between *NCU-G1*$^{gt/gt}$ and WT livers are given for each time-point for the selected genes: **(A)** *MMP-2*; matrix metalloproteinases-2, **(B)** *MMP-9*, **(C)** *TIMP-1*; tissue inhibitors of metalloproteinases-1, **(D)** *S100A8*; S100 calcium binding protein A8, **(E)** *TGF-β1*; transforming growth factor-β1, **(F)** α-*SMA*; α-smooth muscle actin, and **(G)** *Col1α1*; Collagen type I α 1. (n=4). Stars indicate statistical significance (*p $\leq$ 0.05, **p $\leq$ 0.05, ***p $\leq$ 0.05).

4.3.4 Gelatine zymography

The homogenized samples (Ch. 3.2.1) were loaded on a zymography-gel (Ch. 3.2.6) and figure 4.8A shows the gelatinase activity in WT and *NCU-G1*$^{gt/gt}$ liver for each age. The WT mice did not express detectable levels of gelatinase activity at any age point (figure 4.8A), while the *NCU-G1*$^{gt/gt}$ did express different degrees of MMP-9 (92 kDa) activity at all age points, with the highest gelatinase activity at 4.5 months of age. The gel presenting all ages was used to observe the difference in MMP-9 activity between the different time-points. (figure 4.8B).

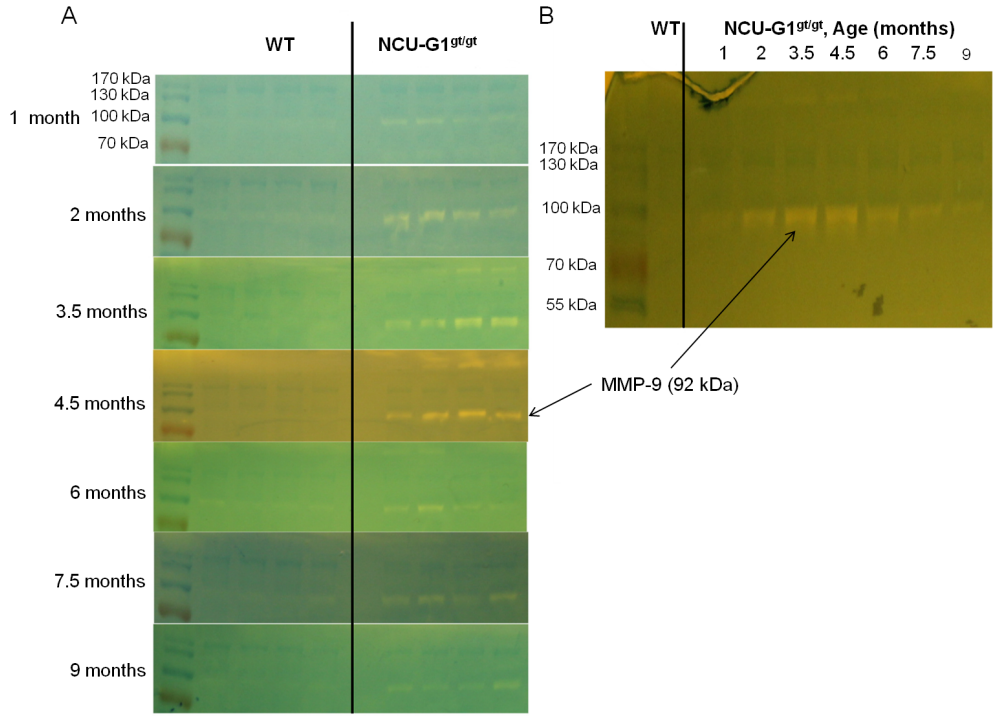

Figure 4.8: **Detection of active gelatinases in *NCU-G1*$^{gt/gt}$ and WT mice liver.**

Figure 4.8: Homogenized liver samples from *NCU-G1*$^{gt/gt}$ and WT mice at different ages were separated on a zymography gel, and the gelatinase activity detected. **(A)** The expression of gelatinases for all investigated ages in *NCU-G1*$^{gt/gt}$ and WT mice liver(n=4). **(B)** A comparison of the expression of gelatinases in *NCU-G1*$^{gt/gt}$ mice livers, between the different age-points.

4.4 NaHS pilot study

4.4.1 Visible change in liver appearance

The 4.5 months old NaHS treated animals displayed a less aggressive liver condition after treatment. There were no visible difference in the appearance of the WT mice livers. The *NCU-G1*$^{gt/gt}$ mice livers lost some of their discoloration and the shape of the livers became less dented and the edges more smooth after treatment (figure 4.9).

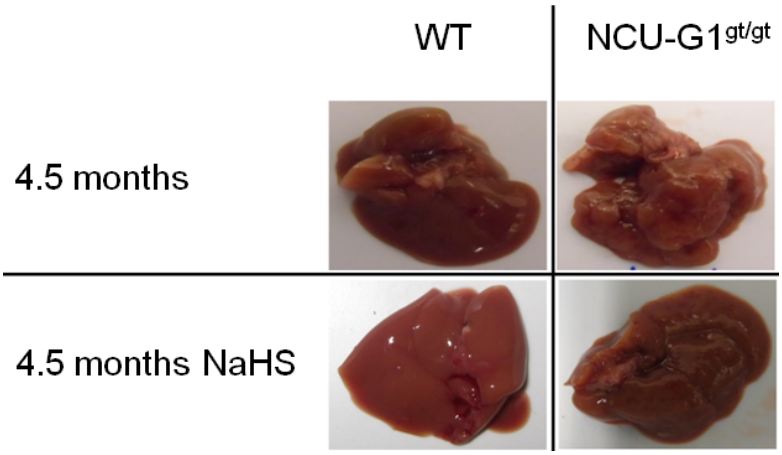

Figure 4.9: **Indication of visible attenuation in NaHS treated mice.** *NCU-G1*$^{gt/gt}$ and WT mice, 3.5 months old, were treated with sodium hydrogen sulfide (NaHS) for 30 days. After treatment the mice were terminated and the livers collected. The the difference in visible development of the fibrosis in WT and *NCU-G1*$^{gt/gt}$ NaHS treated and non-treated mice, was detected by investigating the difference in color change and structure of the livers.

4.4.2 Liver hydroxyproline levels

The samples from the NaHS treated animals was treated in the same way as control samples (Ch. 4.3.2). Figure 4.10 shows the hydroxyproline content in the 4.5 months non-treated and NaHS-treated animals.

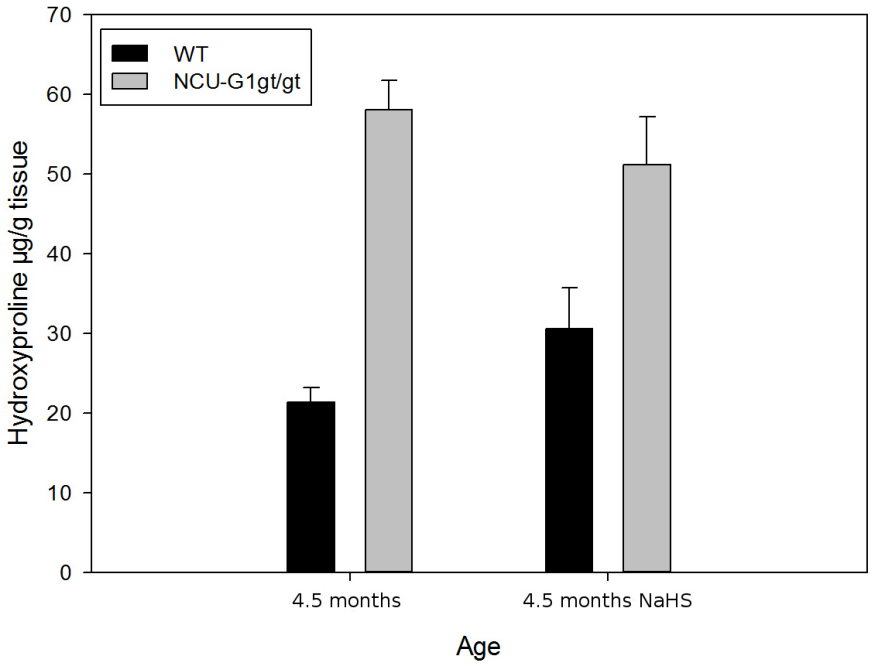

Figure 4.10: **Liver hyrdoxyproline content in NaHS treated and untreated mice.** Powdered liver samples from NaHS; sodium hydrogen sulfide treated and control *NCU-G1*$^{gt/gt}$ and WT mice were hydrolysed in strong acid, and the hydroxyproline levels measured with QuickZymes hydroxyproline kit. The hydroxyproline content in the livers (hydroxyproline μg/g wet tissue) are shown for the treated (n=3) and control (n=4), WT and *NCU-G1*$^{gt/gt}$ mice livers.

The NaHS treated animals showed a tendency to decrease in hydroxyproline content in the liver, but no significant decrease. There was a tendency that the differences in hydroxyproline content between WT and *NCU-G1*$^{gt/gt}$ animals was smaller for the NaHS-treated animals then the non-treated animals, with a difference of 20.6 g hydroxyproline/g wet tissue between the WT and *NCU-G1*$^{gt/gt}$ in the treated animals against a difference of 30.7 g hydroxyproline/g tissue between the WT and *NCU-G1*$^{gt/gt}$ in the non treated animals.

4.4.3 Gelatine zymography

The samples from the NaHS treated animals were treated as described in Ch. 4.3.4. Figure 4.11 shows the NaHS treated and non-treated WT and *NCU-G1*$^{gt/gt}$ animals.

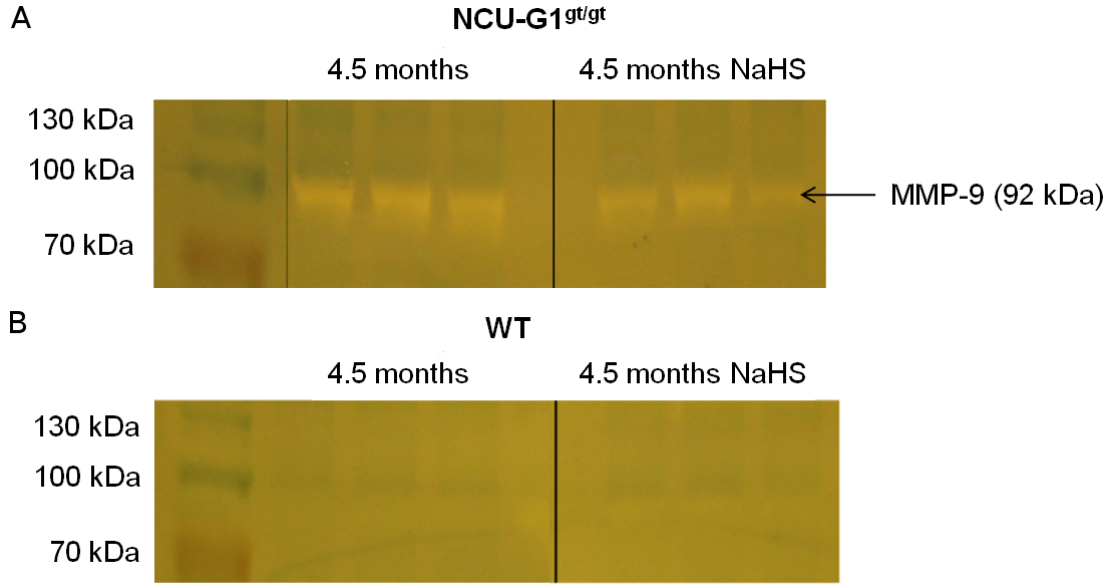

Figure 4.11: **Detection of active gelatinases in NaHS treated and untreated mice.** Homogenized liver samples from NaHS; sodium hydrogen sulfide treated and control *NCU-G1*$^{gt/gt}$ and WT mice were separated on a gelatine zymography gel, and the gelatinase activity detected. The activity of gelatinases for NaHS treated (n=3) and control (n=4) for **(A)** *NCU-G1*$^{gt/gt}$ and **(B)** WT mice livers are shown. MMP-9; matrix metalloproteinases-9.

The expression of MMP-9 has decreased to some extent in the NaHS treated *NCU-G1*$^{gt/gt}$ animals. The NaHS treatment does not increase the protein activity of the gelatinases in the WT animals to a detectable level (figure 4.11).

4.4.4 qRT-PCR analyses of genes of interest

The NaHS treated animal samples were treated similar to the samples from the non-treated animals (Ch. 4.3.3) and the gene expression was compared between the 4.5 month old NaHS-treated and non-treated animals (figure 4.12).

Of the genes tested there was a tendency that the genes *MMP-9*, *TIMP1*, *α-SMA*, *Col1α1* (figure 4.12A) and *S100A8* (figure 4.12B) became less up-regulated after treatment in *NCU-G1*$^{gt/gt}$ liver. The expression of *TGF-β1* and

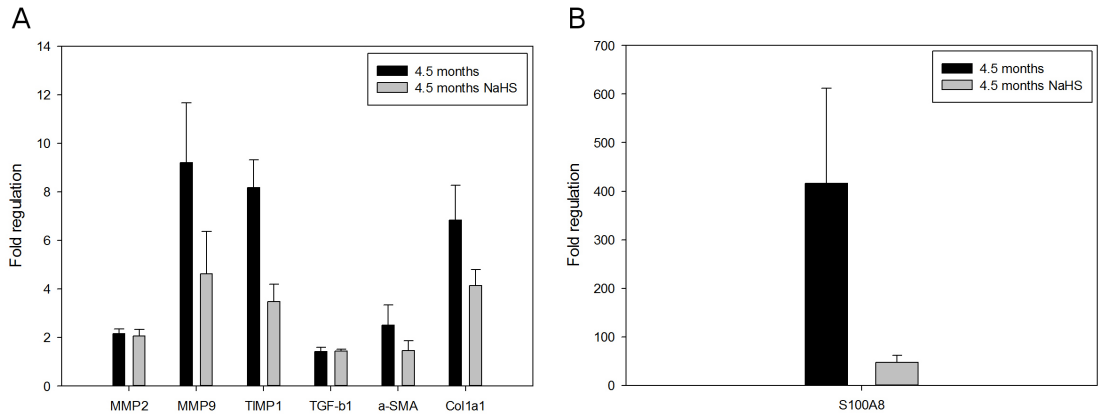

Figure 4.12: **Gene expression analysis of NaHS treated mouse liver.** NaHS; sodium hydrogen sulfide treated and control mice liver samples were investigated with quantitative real-time polymerases chain reaction. The fold relative expression between *NCU-G1*$^{gt/gt}$ and WT mice for the NaHS (n=3) and control (n=4) livers are shown for the genes **(A)** *MMP-2*; matrix metalloproteinases-2, *MMP-9*, *TIMP1*; tissue inhibitors of metalloproteinases-1, *TGF-β1*; transforming growth factor-β1, *α-SMA*; α-smooth muscle actin, *Col1α1*; Collagen type I α 1 and **(B)** *S100A8*; S100 calcium binding protein A8. The results indicate a decrease in expression of the fibrogenic genes in *NCU-G1*$^{gt/gt}$ liver after NaHS treatment.

MMP-2 showed no apparent difference in expression between the NaHS-treated and non-treated *NCU-G1*$^{gt/gt}$ animals. NaHS treatment showed no affect on the gene expression in WT livers (data not shown).

4.5 LC3-Western blot

Mice, 4.5 months old, were starved for 24 hours to induce autophagy, and then terminated (Ch. 3.3.2). Protein samples were made (Ch. 3.2.1), and the samples, together with samples from 4.5 months old control mice, were fractionated on a SDS-PAGE gel (Ch. 3.2.4), and analyzed by Western blotting (Ch. 3.2.5). Microtubuleassociated protein light chain 3 (LC3) is a protein that specifically associates with autophagosome membranes. LC3 is widely used to monitor autophagy, and is detected as two bands on an immunoblot, LC3-I (16 kDa) and LC3-II (14 kDa) [150, 151]. The number of autophagosomes correlate with the amount of LC3II, and is a good indicator of the formation of autophagosomes [150].

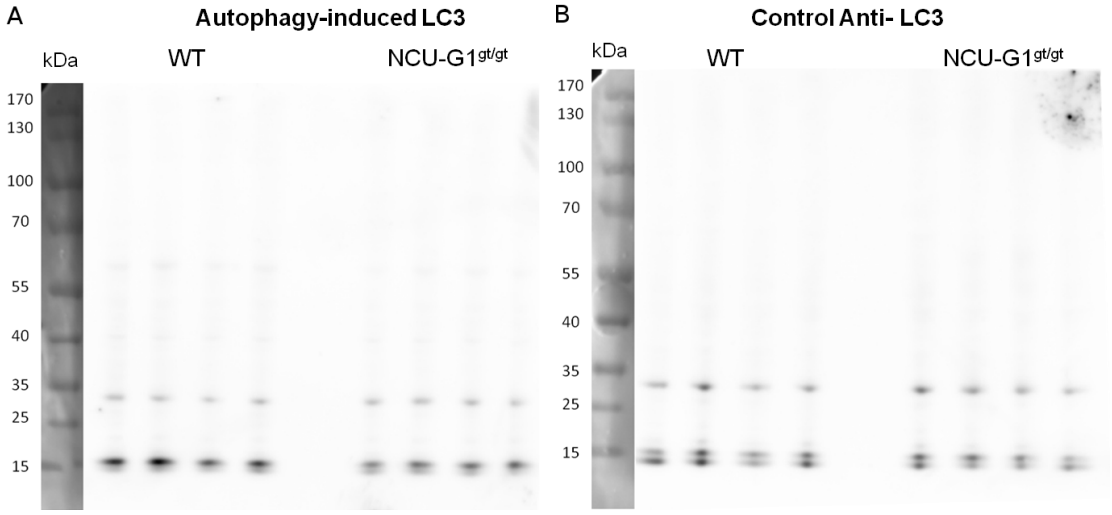

Figure 4.13: **Western blot analysis of autophagy induced mice liver.** 4.5 months old mice were starved for 24 hours to induce autophagy, and liver protein samples from, **(A)** autophagy induced and **(B)** control, *NCU-G1*$^{gt/gt}$ and WT mice,(n=4) were investigated by Western blot analysis with anti-LC3 antibody, which detected LC3-I (16 kDa) and LC3-II (14 kDa).

Control animals did not differ in their expression of LC3 as shown in figure 4.13. There was a tendency to a higher LC3 expression in the WT mice than in the *NCU-G1*$^{gt/gt}$ mice after autophagy-induction. Detection of β-actin as a housekeeping gene was not successful after stripping of the membrane, and quantification could not be performed (supplementary figure D.1).

Chapter 5

Discussion

5.1 Weight study

The number of cage inhabitants has been shown to be a factor which might influence mice weight gain [152]. We observed a deviation in weight gain between the cages with 1 to 3 inhabitants compared to cages with 4 or 5 individuals, for both males and females, independent of the genotype. This may be due to the fact that mice are social animals and should, wherever possible, be maintained in stable, harmonious social groups. It is not advised to house mice individually, unless there are special circumstances such as highly aggressive individuals or strains [152]. The observed deviation was more prominent among the females, which gained more weight in general when housed in cages with less than 4 inhabitants. This prominent weight gain observed in females but not in males may be because pair housing (two individuals per cage) can lead to aggression and stress, and this factor has a stronger influence on males than females [152].

NCU-G1 was earlier defined as a co-activator for PPAR-α which is a major regulator of lipid metabolism [112, 153]. We investigated the weight development and food efficiency of the *NCU-G1*$^{gt/gt}$ and WT mice, and discovered that there were no differences between them. Treatment with PPAR-α agonists has been shown to induce the expression of fatty-acid metabolic enzymes, which would indicate a slower weight gain in mice with decreased PPAR-α activation [154]. The lack of difference in weight gain and food efficiency, however, indicates that the metabolism in the *NCU-G1*$^{gt/gt}$ mice is not influenced as a result of the lack of this PPAR-α co-activator.

5.2 Progression of liver damage

The development of liver fibrosis was analysed in livers from *NCU-G1*$^{gt/gt}$ and WT mice collected at different ages. We observed a development of discolored patches and a dented shape in the *NCU-G1*$^{gt/gt}$ mice livers, not present in the WT. The formation of scar tissue and accumulation of fibrotic ECM in the space of Disse may lead to portal hypertension [1], and this often leads to enlargement of the spleen as a result of an increase in splenic blood flow [155]. We observed an enlargement of the spleen in the *NCU-G1*$^{gt/gt}$ mice, probably as a secondary effect of the fibrosis.

The hydroxyproline content of the WT mice is uniform throughout the study and sets a baseline for the amount of connective tissue and ECM present in normal healthy livers. Hydroxyproline content in the livers spans from 13.30 to 21.39 μg/g tissue in our studies. The hydroxyproline content in the *NCU-G1*$^{gt/gt}$ mice livers is significantly higher than for the WT mice at all ages studied, with a maximum of 58.06 μg hydroxyproline/g tissue at the age of 4.5 months. Previous studies with fibrosis models have reported several measurements of hydroxyproline in fibrotic livers [156–158]. CCl_4 induction of liver fibrosis in mice resulted in values as high as 846 μg hydroxyproline/g tissue, just after treatment, reaching a peak of 1188 μg hydroxyproline/g tissue two weeks after treatment was terminated, in contrast to 189 μg hydroxyproline/g tissue in livers from untreated mice. This is approximately an increase of 3.5 times of hydroxyproline between the CCl_4 treated and untreated mice just after treatment was terminated [156]. A study in rats with BDL induced fibrosis gave the values 452 μg hydroxyproline/g tissue in contrast to 132 μg hydroxyproline/g tissue if sham operated, which is approximately a 2.5 times increase in hydroxyproline levels between the BDL and sham mice [157].

It has been shown that a KO mouse model with a hepatocyte-specific ablation of B-cell lymphoma-extra large *Bcl-*x_L, spontaneously develops fibrosis over a longer time period. The progressive development of the fibrosis spans over several months, and displays approximately a doubling in hydroxyproline level at its most fibrotic state compared to control mice. The measured hydroxyproline levels in this model showed a more modest increase in hydroxyproline content compared to other fibrosis models such as CCl_4 and BDL [158]. The *NCU-G1*$^{gt/gt}$ mice also develop fibrosis over a longer period of time, and our mice have an increase in hy-

droxyproline level of approximately 1.7 times compared to the WT at their most fibrotic state. The lower increase in hydroxyproline in our mice compared to studies with BDL and CCl_4 induced fibrosis, may be ascribed to the less dramatic and slower development of fibrosis in the *NCU-G1*$^{gt/gt}$ model organism. In comparison with the hepatocyte *Bcl-*x_L KO mouse the *NCU-G1*$^{gt/gt}$ mouse have a prominent inflammation, which is not observed in *Bcl-*x_L KO. The fact that the *NCU-G1*$^{gt/gt}$ mouse develops a slightly more severe fibrosis than *Bcl-*x_L KO mouse may be due to the contribution of inflammatory signals on fibrosis progression [5].

Hydroxyproline is regarded as a good measurement of the grade and severity of fibrosis [159–163], but the method is questioned because of the observed sample variability [159]. Furthermore, the distribution of hydroxyproline in the liver is uneven, and it is reported that different samples from the same liver give variability in hydroxyproline measurements [160]. The samples used for our hydroxyproline measurements were liver powder (i.e. mix of powdered whole liver), resulting in less variation between measurements compared to samples taken by biopsy. The lack of spread in the data suggests that the "sampling problem" is not an issue when working with homogenates from powdered whole liver.

A study conducted in the *Mdr2*$^{-/-}$ mice reported a similar pattern of up- and down-regulation of the genes TGF-β1, α-SMA and MMP-2 [163], as observed in our animals. They propose that the reason for the observed decrease in expression of these genes in the *Mdr2*$^{-/-}$ mouse, is a result of reduced autoinduction of TGF-β1, given by the decreased responsiveness to TGF-β1 in activated HSC [14].

TGF-β1 was up-regulated in *NCU-G1*$^{gt/gt}$ liver at all time-points (e.g. 1, 2, 3.5, 4.5, 6, 7.5 and 9 months), and the expression levels peaked at 3.5 months indicating that the fibrogenesis is most active at this time-point [163]. We also observed a small peak in expression at 7.5 months for all the genes except α-SMA. The changes in expression levels of all the genes investigated followed that of TGF-β1 mRNA expression except TIMP1 which was consistently up-regulated at all time-points.

TGF-β1 promotes expression of genes leading to production of ECM components, such as TIMP-1 and MMP-2, and suppresses the activity of genes that degrade ECM such as some of the class 1 MMPs, the collagenases [164–166].

The gelatinases MMP-2 and MMP-9 have been shown to activate, in addition to being influenced by, TGF-β [166,167]. The regulation of both gelatinases follows

a similar curve as TGF-β1 peaking at the age of 3.5 months in the *NCU-G1*$^{gt/gt}$ liver.

α-SMA is an indicator of stellate cell activation, a marker for fibrosis progression [168] and its expression has been shown to be induced by TGF-β1 [169]. The observed α-SMA expression does not have the small increase in expression at 7.5 months as some of the other genes, and it is proposed that the need for α-SMA as an activation marker is only necessary in early stages of fibrogenesis [163]. This may be the cause of the lack of increase in α-SMA expression in the *NCU-G1*$^{gt/gt}$ mice at the time-point 7.5 months.

Col1α1 expression in *NCU-G1*$^{gt/gt}$ liver increases in the same way as TGF-β1 expression, however the expression of Col1α1 peaks at 4.5 months, which is approximately one month later than the peak expression of the other genes. TGF-β1 is shown to induce the accumulation of H_2O_2 in HSC after activation, and this accumulation is directly involved in the up-regulation of Col1α1 [170]. The late peak in up-regulation of Col1α1 may be due to accumulation of ROS in the HSC, which drives the Col1α1 expression forward even after TGF-β1 levels have decreased [170].

S100A8 functions as a potent chemokine for neutrophil recruitment to inflammation sites [171, 172], and plays an important role in nonspecific and immune mediated responses [173]. The decrease in S100A8 after 4.5 months indicates that the level of inflammation in *NCU-G1*$^{gt/gt}$ liver decreases.

TIMP-1 is up-regulated at all ages in the *NCU-G1*$^{gt/gt}$ mice relative to WT. Earlier studies state that the continuous over-expression of TIMP-1 in a mouse model most likely is a central determinant of fibrosis progression as TIMP-1 inhibits most of the MMPs, which are essential for degradation of ECM [79,163,174].

The amount of active MMP-9 increases to a maximum at 4.5 months of age in the *NCU-G1*$^{gt/gt}$ liver, and then decreases as the mice age, while the WT samples show no detectable protein activity of MMPs at any time point. The gelatinases MMP-2 and MMP-9 mainly digest the denatured form of collagen, gelatine [76]. It has been reported that MMP-2 is able to degrade not only gelatine, but also native type I collagen, and MMP-2 is shown to function as a pro-fibrotic protein [77, 78]. MMP-2 and MMP-9 have been shown to be regulated at several levels (e.g. transcription, translation, and post translational modifications) [147], and it is the expression of active MMP proteins that influences the ECM composition [47, 76, 77]. Gelatine zymography is highly sensitive to MMP-2, down to levels

of 10 pg [175]. Our inability to detect MMP-2 in our samples may be because MMP-2 is present as a pro-enzyme, and not as an active protein in our samples. It may also be caused by the continued expression of TIMP-1, which has been shown to inhibit apoptosis of activated HSC by suppressing MMP activity [176].

The gene expression of TGF-β1, Col1α1, α-SMA, MMP-2, MMP-9 and S100A8 show the same decrease in the fibrotic state as the hydroxyproline and gelatine zymography measurements after the time-points 3.5 and 4.5 months. This suggests that the fibrosis is reversed to some degree after the mice reach the age of 4.5 months.

In a study of the impact of HSC senescence on liver fibrosis, it is proposed that senescence of HSC limits liver fibrosis by promoting down-regulation of ECM components and up-regulation of ECM degrading enzymes such as the MMPs. It was shown that the senescent HSC produce signals that attract immune cells leading to the clearance of the activated HSC from the tissue. Furthermore, the study indicates that the senescent HSC are selectively targeted by NK cells for NK cell mediated clearance [37].

The decrease in fibrosis, at the age 4.5 months observed in *NCU-G1*$^{gt/gt}$ mice, may be due to senescence of the activated HSC in the liver. There is a decrease in ECM components shown by the hydroxyproline content of the livers and the expression of Col1α1. The decrease in up-regulation observed in the known marker of active HSC, α-SMA, and the other pro-fibrotic genes investigated (e.g. TGF-β1, MMP-2, MMP-9 and S100A8), indicates that there is a decrease in the number of activated HSC in the liver. The decrease in protein expression of active MMP-9 may indicate that there is less of its substrate, gelatine (i.e the denatured form of collagen [76]), in the liver. The expression of MMP-9 is tightly regulated by inflammatory-cells and cytokines [177]. The recruitment of immune cells to the fibrotic sites may regulate the expression of MMP-9. NK cells participate in the clearance of activated HSC [24], hence the reversion of fibrosis in *NCU-G1*$^{gt/gt}$ animals may be due to the NK mediated clearance of the senescent activated HSC. NK mediated apoptosis is important for clearance of activated HSC in the liver [36], but apoptosis also induces activation of HSC and fibrosis [39]. The observed increase in hydroxyproline content and expression of TGF-β1, MMP-2, MMP-9, S100A8 and Col1α1 at 7.5 months may be due to NK cell mediated apoptosis of the activated HSC after the age 4.5 months. This is because the amount of apoptotic

bodies in the liver activate more HSC, which stop the reversion of fibrosis and increase the production of ECM components.

5.3 NaHS pilot study

The *NCU-G1*$^{gt/gt}$ mouse may serve as a fibrosis model organism. In contrast to other fibrosis models like CCl_4, TAA and BDL, which develop fibrosis within weeks of treatment [105,107], the liver fibrosis in *NCU-G1*$^{gt/gt}$ mice is spontaneous, develops over time and has a less dramatic fibrosis development, as can be seen from the maximum hydroxyproline content in our animals. In comparison with the *Mdr2*$^{-/-}$ mouse model, which displays the same gene regulation pattern of TGF β1, α-SMA, MMP-2 and TIMP-1 [109], the *NCU-G1*$^{gt/gt}$ mouse does not develop carcinoma until late in its lifespan [unpublished]. The *NCU-G1*$^{gt/gt}$ mouse model has the potential to be used for studying the development of fibrosis, for drug trials and development, and may be able to induce more severe cases of fibrosis if challenged with carcinogenic or fibrotic agents. Older animals may also be used to study development of HCC [unpublished].

The development of a rodent model organism for fibrosis is crucial to achieve a better understanding of the mechanisms behind fibrosis, and to be able to design new anti-fibrotic drugs. Presently, there are no experimental models on the marked, which mimic human liver fibrosis and its development [103].

To be able to establish the *NCU-G1*$^{gt/gt}$ mouse as a new model organism for liver fibrosis, the response to anti-fibrotic treatment had to be clarified. A pilot study was performed, spanning a period of 30 days, on 3.5 months old mice with NaHS, which is a known anti-fibrotic compound [96, 97].

The NaHS treated *NCU-G1*$^{gt/gt}$ mice show attenuation of the fibrotic condition after 30 days of NaHS treatment, the livers became less discolored and the shape less dented with smoother edges than the untreated livers. The treatment resulted in a tendency towards lower levels of hydroxyproline in *NCU-G1*$^{gt/gt}$ liver compared to the untreated mice, but no significant results were obtained. This may be due to the small test group (n=3) and the short time period of administration. The qRT-PCR and gelatine zymography data of the NaHS treated and untreated mice show a tendency to a decrease in the expression of most genes at the mRNA level and of active MMP-9 at protein level in the NaHS treated mice. MMP-2 is

not detectable as an active protein in neither NaHS treated nor untreated mice. Several studies of NaHS administration to fibrosis model organisms show attenuation of fibrosis and collagen protein expression [178, 179]. Work with cell cultures show that NaHS inhibits proliferation and induces cell cycle arrest and apoptosis in activated HSC [178].

The up-regulation of TGF-β1 and MMP-2 did not seem to differ between the NaHS treated and untreated *NCU-G1*$^{gt/gt}$ mice. HSC are not the only cell type producing TGF-β1 and MMPs in the liver, KC also express these proteins and aid in the activation of HSC and fibrosis progression [1]. NaHS specifically induces apoptosis in HSC without affecting the number of active KC in the liver [101]. The lack of reduction of TGF-β1 and MMP-2 expression levels after NaHS treatment of *NCU-G1*$^{gt/gt}$ mice, most probably, is a result of the continued production of TGF-β1 and MMP-2 by the KC. HSC have been shown to be less responsive to TGF-β1 after activation [14], and this may also be a reason for the lack of reduction of TGF-β1 after NaHS treatment.

5.4 Autophagy impairment

The Western blot analyses of LC3, a commonly used autophagy marker [150], do not indicate impairment of autophagy in the autophagy-induced *NCU-G1*$^{gt/gt}$ mice compared with the *NCU-G1*$^{gt/gt}$ control mice.

LSD have been shown to be caused by dysfunction and mutations in the proteins regulating lysosomal function, leading to intralysosomal accumulation of undegraded materials. It has been shown that the liver is one of the organs often affected by LSD [118, 122]. LSD often affect the autophagic pathway, resulting from impaired fusion between autophagosomes and undegraded material-laden lysosomes, leading to accumulation of autophagic substances in the cell [129, 180]. The lack of NCU-G1 in the lysosomal membrane may impair lysosomal function which leads to the development of liver fibrosis. The data cannot in its current state give an indication of this, and the possibility of LSD being the fibrotic inducer in the *NCU-G1*$^{gt/gt}$ mice must be further investigated.

Conclusion and future aspects

The aim for this study was to investigate the progression of liver fibrosis in the *NCU-G1*$^{gt/gt}$ mouse and the response to anti-fibrotic treatment with NaHS, in order to establish the *NCU-G1*$^{gt/gt}$ mouse as a model organism, and to explore some possible causes for the development of the liver fibrosis in the *NCU-G1*$^{gt/gt}$ mice.

The study was divided into the following sub-projects:

- Do the *NCU-G1*$^{gt/gt}$ mice have a metabolic disorder as a reaction to the lack of *NCU-G1*, that is reflected in their weight gain and food consumption?

  Main result:
  There was no difference in weight gain and food consumption between the *NCU-G1*$^{gt/gt}$ and WT mice that suggested the presence of metabolic disorder caused by the lack of NCU-G1 as a co-activator for PPAR-α.

- How does the fibrosis progress in the *NCU-G1*$^{gt/gt}$ mice?

  Main result:
  The liver fibrosis in *NCU-G1*$^{gt/gt}$ mice develops until the mice reach 4.5 months of age, after this time-point the fibrosis seems to revert to some degree, but not to complete reversion and clearance of the fibrosis.

- Do the *NCU-G1*$^{gt/gt}$ mice respond to treatment with anti-fibrotic agents such as NaHS?

  Main result:
  The *NCU-G1*$^{gt/gt}$ mice have a tendency to attenuation of the fibrotic condi-

tion after treatment with the anti-fibrotic agent NaHS.

- Do the *NCU-G1*$^{gt/gt}$ mice have impairment of the autophagic pathway that may indicate lysosomal storage disease?

  Main result:
  This issue is still unclear due to the lack of opportunity to quantify the data, hence the possibility for LSD to be the cause of fibrotic progression should be investigated further.

Future aspects:

- The gene expression analyses should be expanded with other MMPs such as the collagenases; MMP-1, MMP-8 and MMP-13, and TIMP-2, to get a more complete picture of the regulation of the ECM modifying proteins.
- Protein analyses of the MMPs should be conducted to investigate the regulation of protein expression in the fibrotic livers.
- The gelatine zymography should be repeated and quantified, and the method should be modified to detect the pro-MMP-9 and pro-MMP-2 proteins in addition to the active MMP-9 and MMP-2.
- The Western blot analyses with LC3 should be repeated with different β-actin antibodies, or another housekeeping gene, and a milder stripping method.
- The treatment with NaHS should be replicated with a larger number of biological replicas.
- There would be of interest to investigate if the activated HSC get senescent in the fibrotic liver.

Bibliography

[1] J. Guo and S. L. Friedman. Hepatic fibrogenesis. *Semin. Liver Dis.*, 27(4):413–426, Nov 2007.

[2] R. Bataller and D. A. Brenner. Liver fibrosis. *J. Clin. Invest.*, 115(2):209–218, Feb 2005.

[3] S. L. Friedman. Hepatic fibrosis – overview. *Toxicology*, 254(3):120–129, Dec 2008.

[4] G. Fattovich, T. Stroffolini, I. Zagni, and F. Donato. Hepatocellular carcinoma in cirrhosis: incidence and risk factors. *Gastroenterology*, 127(5 Suppl 1):35–50, Nov 2004.

[5] S. L. Friedman. Molecular regulation of hepatic fibrosis, an integrated cellular response to tissue injury. *J. Biol. Chem.*, 275(4):2247–2250, Jan 2000.

[6] T. Kisseleva and D. A. Brenner. Mechanisms of fibrogenesis. *Exp. Biol. Med. (Maywood)*, 233(2):109–122, Feb 2008.

[7] S. L. Friedman. Hepatic stellate cells: protean, multifunctional, and enigmatic cells of the liver. *Physiol. Rev.*, 88(1):125–172, Jan 2008.

[8] A. Schulze-Krebs, D. Preimel, Y. Popov, R. Bartenschlager, V. Lohmann, M. Pinzani, and D. Schuppan. Hepatitis C virus-replicating hepatocytes induce fibrogenic activation of hepatic stellate cells. *Gastroenterology*, 129(1):246–258, Jul 2005.

[9] M. Pinzani. PDGF and signal transduction in hepatic stellate cells. *Front. Biosci.*, 7:d1720–1726, Aug 2002.

[10] F. Marra, G. Grandaliano, A. J. Valente, and H. E. Abboud. Thrombin stimulates proliferation of liver fat-storing cells and expression of monocyte

chemotactic protein-1: potential role in liver injury. *Hepatology*, 22(3):780–787, Sep 1995.

[11] E. Patsenker, Y. Popov, M. Wiesner, S. L. Goodman, and D. Schuppan. Pharmacological inhibition of the vitronectin receptor abrogates PDGF-BB-induced hepatic stellate cell migration and activation in vitro. *J. Hepatol.*, 46(5):878–887, May 2007.

[12] J. S. Lee, N. Kang Decker, S. Chatterjee, J. Yao, S. Friedman, and V. Shah. Mechanisms of nitric oxide interplay with Rho GTPase family members in modulation of actin membrane dynamics in pericytes and fibroblasts. *Am. J. Pathol.*, 166(6):1861–1870, Jun 2005.

[13] C. Yang, M. Zeisberg, B. Mosterman, A. Sudhakar, U. Yerramalla, K. Holthaus, L. Xu, F. Eng, N. Afdhal, and R. Kalluri. Liver fibrosis: insights into migration of hepatic stellate cells in response to extracellular matrix and growth factors. *Gastroenterology*, 124(1):147–159, Jan 2003.

[14] S. Dooley, B. Delvoux, B. Lahme, K. Mangasser-Stephan, and A. M. Gressner. Modulation of transforming growth factor beta response and signaling during transdifferentiation of rat hepatic stellate cells to myofibroblasts. *Hepatology*, 31(5):1094–1106, May 2000.

[15] H. Sprenger, A. Kaufmann, H. Garn, B. Lahme, D. Gemsa, and A. M. Gressner. Induction of neutrophil-attracting chemokines in transforming rat hepatic stellate cells. *Gastroenterology*, 113(1):277–285, Jul 1997.

[16] F. Marra, A. J. Valente, M. Pinzani, and H. E. Abboud. Cultured human liver fat-storing cells produce monocyte chemotactic protein-1. Regulation by proinflammatory cytokines. *J. Clin. Invest.*, 92(4):1674–1680, Oct 1993.

[17] M. Pinzani and F. Marra. Cytokine receptors and signaling in hepatic stellate cells. *Semin. Liver Dis.*, 21(3):397–416, Aug 2001.

[18] D. C. Rockey. Vascular mediators in the injured liver. *Hepatology*, 37(1):4–12, Jan 2003.

[19] J. P. Iredale. Cirrhosis: new research provides a basis for rational and targeted treatments. *BMJ*, 327(7407):143–147, Jul 2003.

[20] M. Okuno, S. Kojima, K. Akita, R. Matsushima-Nishiwaki, S. Adachi, T. Sano, Y. Takano, K. Takai, A. Obora, I. Yasuda, Y. Shiratori, Y. Okano, J. Shimada, Y. Suzuki, Y. Muto, and Y. Moriwaki. Retinoids in liver fibrosis and cancer. *Front. Biosci.*, 7:d204–218, Jan 2002.

[21] O. Vinas, R. Bataller, P. Sancho-Bru, P. Gines, C. Berenguer, C. Enrich, J. M. Nicolas, G. Ercilla, T. Gallart, J. Vives, V. Arroyo, and J. Rodes. Human hepatic stellate cells show features of antigen-presenting cells and stimulate lymphocyte proliferation. *Hepatology*, 38(4):919–929, Oct 2003.

[22] Y. H. Paik, R. F. Schwabe, R. Bataller, M. P. Russo, C. Jobin, and D. A. Brenner. Toll-like receptor 4 mediates inflammatory signaling by bacterial lipopolysaccharide in human hepatic stellate cells. *Hepatology*, 37(5):1043–1055, May 2003.

[23] P. Brun, I. Castagliuolo, M. Pinzani, G. Palu, and D. Martines. Exposure to bacterial cell wall products triggers an inflammatory phenotype in hepatic stellate cells. *Am. J. Physiol. Gastrointest. Liver Physiol.*, 289(3):G571–578, Sep 2005.

[24] W. Z. Mehal. Activation-induced cell death of hepatic stellate cells by the innate immune system. *Gastroenterology*, 130(2):600–603, Feb 2006.

[25] M. Bilzer, F. Roggel, and A. L. Gerbes. Role of Kupffer cells in host defense and liver disease. *Liver Int.*, 26(10):1175–1186, Dec 2006.

[26] S. S. Zhan, J. X. Jiang, J. Wu, C. Halsted, S. L. Friedman, M. A. Zern, and N. J. Torok. Phagocytosis of apoptotic bodies by hepatic stellate cells induces NADPH oxidase and is associated with liver fibrosis in vivo. *Hepatology*, 43(3):435–443, Mar 2006.

[27] W. R. Jarnagin, D. C. Rockey, V. E. Koteliansky, S. S. Wang, and D. M. Bissell. Expression of variant fibronectins in wound healing: cellular source and biological activity of the EIIIA segment in rat hepatic fibrogenesis. *J. Cell Biol.*, 127(6 Pt 2):2037–2048, Dec 1994.

[28] S. A. Doggrell. The endothelin system and its role in acute myocardial infarction. *Expert Opin. Ther. Targets*, 8(3):191–201, Jun 2004.

[29] N. Sedlaczek, J. D. Jia, M. Bauer, H. Herbst, M. Ruehl, E. G. Hahn, and D. Schuppan. Proliferating bile duct epithelial cells are a major source of connective tissue growth factor in rat biliary fibrosis. *Am. J. Pathol.*, 158(4):1239–1244, Apr 2001.

[30] N. Kinnman, R. Hultcrantz, V. Barbu, C. Rey, D. Wendum, R. Poupon, and C. Housset. PDGF-mediated chemoattraction of hepatic stellate cells by bile duct segments in cholestatic liver injury. *Lab. Invest.*, 80(5):697–707, May 2000.

[31] R. Kalluri and E. G. Neilson. Epithelial-mesenchymal transition and its implications for fibrosis. *J. Clin. Invest.*, 112(12):1776–1784, Dec 2003.

[32] M. Beaussier, D. Wendum, E. Schiffer, S. Dumont, C. Rey, A. Lienhart, and C. Housset. Prominent contribution of portal mesenchymal cells to liver fibrosis in ischemic and obstructive cholestatic injuries. *Lab. Invest.*, 87(3):292–303, Mar 2007.

[33] T. Kisseleva, H. Uchinami, N. Feirt, O. Quintana-Bustamante, J. C. Segovia, R. F. Schwabe, and D. A. Brenner. Bone marrow-derived fibrocytes participate in pathogenesis of liver fibrosis. *J. Hepatol.*, 45(3):429–438, Sep 2006.

[34] N. C. Henderson and J. P. Iredale. Liver fibrosis: cellular mechanisms of progression and resolution. *Clin. Sci.*, 112(5):265–280, Mar 2007.

[35] T. I. Novobrantseva, G. R. Majeau, A. Amatucci, S. Kogan, I. Brenner, S. Casola, M. J. Shlomchik, V. Koteliansky, P. S. Hochman, and A. Ibraghimov. Attenuated liver fibrosis in the absence of B cells. *J. Clin. Invest.*, 115(11):3072–3082, Nov 2005.

[36] S. Radaeva, R. Sun, B. Jaruga, V. T. Nguyen, Z. Tian, and B. Gao. Natural killer cells ameliorate liver fibrosis by killing activated stellate cells in NKG2D-dependent and tumor necrosis factor-related apoptosis-inducing ligand-dependent manners. *Gastroenterology*, 130(2):435–452, Feb 2006.

[37] V. Krizhanovsky, M. Yon, R. A. Dickins, S. Hearn, J. Simon, C. Miething, H. Yee, L. Zender, and S. W. Lowe. Senescence of activated stellate cells limits liver fibrosis. *Cell*, 134(4):657–667, Aug 2008.

[38] A. Melhem, N. Muhanna, A. Bishara, C. E. Alvarez, Y. Ilan, T. Bishara, A. Horani, M. Nassar, S. L. Friedman, and R. Safadi. Anti-fibrotic activity of NK cells in experimental liver injury through killing of activated HSC. *J. Hepatol.*, 45(1):60–71, Jul 2006.

[39] A. Canbay, S. Friedman, and G. J. Gores. Apoptosis: the nexus of liver injury and fibrosis. *Hepatology*, 39(2):273–278, Feb 2004.

[40] O. Rosmorduc, D. Wendum, C. Corpechot, B. Galy, N. Sebbagh, J. Raleigh, C. Housset, and R. Poupon. Hepatocellular hypoxia-induced vascular endothelial growth factor expression and angiogenesis in experimental biliary cirrhosis. *Am. J. Pathol.*, 155(4):1065–1073, Oct 1999.

[41] M. C. Brahimi-Horn, J. Chiche, and J. Pouyssegur. Hypoxia signalling controls metabolic demand. *Curr. Opin. Cell Biol.*, 19(2):223–229, Apr 2007.

[42] C. Corpechot, V. Barbu, D. Wendum, N. Kinnman, C. Rey, R. Poupon, C. Housset, and O. Rosmorduc. Hypoxia-induced VEGF and collagen I expressions are associated with angiogenesis and fibrogenesis in experimental cirrhosis. *Hepatology*, 35(5):1010–1021, May 2002.

[43] V. Ankoma-Sey, Y. Wang, and Z. Dai. Hypoxic stimulation of vascular endothelial growth factor expression in activated rat hepatic stellate cells. *Hepatology*, 31(1):141–148, Jan 2000.

[44] Y. Q. Wang, J. M. Luk, K. Ikeda, K. Man, A. C. Chu, K. Kaneda, and S. T. Fan. Regulatory role of vHL/HIF-1alpha in hypoxia-induced VEGF production in hepatic stellate cells. *Biochem. Biophys. Res. Commun.*, 317(2):358–362, Apr 2004.

[45] W. I. Jeong, S. H. Do, H. S. Yun, B. J. Song, S. J. Kim, W. J. Kwak, S. E. Yoo, H. Y. Park, and K. S. Jeong. Hypoxia potentiates transforming growth factor-beta expression of hepatocyte during the cirrhotic condition in rat liver. *Liver Int.*, 24(6):658–668, Dec 2004.

[46] S. L. Friedman. Mechanisms of hepatic fibrogenesis. *Gastroenterology*, 134(6):1655–1669, May 2008.

[47] D. Karo-Atar, I. Moshkovits, O. Eickelberg, M. Konigshoff, and A. Munitz. Paired immunoglobulin-like receptor-B inhibits pulmonary fibrosis by suppressing profibrogenic properties of alveolar macrophages. *Am. J. Respir. Cell Mol. Biol.*, 48(4):456–464, Apr 2013.

[48] A. Galli, G. Svegliati-Baroni, E. Ceni, S. Milani, F. Ridolfi, R. Salzano, M. Tarocchi, C. Grappone, G. Pellegrini, A. Benedetti, C. Surrenti, and A. Casini. Oxidative stress stimulates proliferation and invasiveness of hepatic stellate cells via a MMP2-mediated mechanism. *Hepatology*, 41(5):1074–1084, May 2005.

[49] G. E. Arteel. Oxidants and antioxidants in alcohol-induced liver disease. *Gastroenterology*, 124(3):778–790, Mar 2003.

[50] M. Parola and G. Robino. Oxidative stress-related molecules and liver fibrosis. *J. Hepatol.*, 35(2):297–306, Aug 2001.

[51] K. Tomita, G. Tamiya, S. Ando, K. Ohsumi, T. Chiyo, A. Mizutani, N. Kitamura, K. Toda, T. Kaneko, Y. Horie, J. Y. Han, S. Kato, M. Shimoda, Y. Oike, M. Tomizawa, S. Makino, T. Ohkura, H. Saito, N. Kumagai, H. Nagata, H. Ishii, and T. Hibi. Tumour necrosis factor alpha signalling through activation of Kupffer cells plays an essential role in liver fibrosis of non-alcoholic steatohepatitis in mice. *Gut*, 55(3):415–424, Mar 2006.

[52] T. Knittel, C. Dinter, D. Kobold, K. Neubauer, M. Mehde, S. Eichhorst, and G. Ramadori. Expression and regulation of cell adhesion molecules by hepatic stellate cells (HSC) of rat liver: involvement of HSC in recruitment of inflammatory cells during hepatic tissue repair. *Am. J. Pathol.*, 154(1):153–167, Jan 1999.

[53] M. Penz-Osterreicher, C. H. Osterreicher, and M. Trauner. Fibrosis in autoimmune and cholestatic liver disease. *Best Pract Res Clin Gastroenterol*, 25(2):245–258, Apr 2011.

[54] G. M. Hirschfield and E. J. Heathcote. Cholestasis and cholestatic syndromes. *Curr. Opin. Gastroenterol.*, 25(3):175–179, May 2009.

[55] Y. Ilan. Leaky gut and the liver: a role for bacterial translocation in non-alcoholic steatohepatitis. *World J. Gastroenterol.*, 18(21):2609–2618, Jun 2012.

[56] T. M. Bauer, H. Schwacha, B. Steinbruckner, F. E. Brinkmann, A. K. Ditzen, J. J. Aponte, K. Pelz, D. Berger, M. Kist, and H. E. Blum. Small intestinal bacterial overgrowth in human cirrhosis is associated with systemic endotoxemia. *Am. J. Gastroenterol.*, 97(9):2364–2370, Sep 2002.

[57] K. S. Brown, M. J. Keogh, N. Tagiuri, M. J. Grainge, J. S. Presanis, S. D. Ryder, W. L. Irving, J. K. Ball, R. B. Sim, and T. P. Hickling. Severe fibrosis in hepatitis C virus-infected patients is associated with increased activity of the mannan-binding lectin (MBL)/MBL-associated serine protease 1 (MASP-1) complex. *Clin. Exp. Immunol.*, 147(1):90–98, Jan 2007.

[58] K. Paunovic, M. Stojanovic, Z. Dimitrijevic, G. Paunovic, V. Djordjevic, L. Konstantinovic, and S. Kostic. Indirect serum fibrosis markers in hepatitis C virus (HCV) infection. *Med Arh*, 66(4):226–230, 2012.

[59] B. Gangadharan, M. A. Hoeve, J. E. Allen, B. Ebrahimi, S. M. Rhind, B. M. Dutia, and A. A. Nash. Murine gammaherpesvirus-induced fibrosis is associated with the development of alternatively activated macrophages. *J. Leukoc. Biol.*, 84(1):50–58, Jul 2008.

[60] J. J. Egan, A. A. Woodcock, and J. P. Stewart. Viruses and idiopathic pulmonary fibrosis. *Eur. Respir. J.*, 10(7):1433–1437, Jul 1997.

[61] A. Canbay, A. E. Feldstein, H. Higuchi, N. Werneburg, A. Grambihler, S. F. Bronk, and G. J. Gores. Kupffer cell engulfment of apoptotic bodies stimulates death ligand and cytokine expression. *Hepatology*, 38(5):1188–1198, Nov 2003.

[62] S. Y. Proskuryakov, A. G. Konoplyannikov, and V. L. Gabai. Necrosis: a specific form of programmed cell death? *Exp. Cell Res.*, 283(1):1–16, Feb 2003.

[63] H. Malhi, G. J. Gores, and J. J. Lemasters. Apoptosis and necrosis in the liver: a tale of two deaths? *Hepatology*, 43(2 Suppl 1):31–44, Feb 2006.

[64] P. P. Simeonova, R. M. Gallucci, T. Hulderman, R. Wilson, C. Kommineni, M. Rao, and M. I. Luster. The role of tumor necrosis factor-alpha in liver toxicity, inflammation, and fibrosis induced by carbon tetrachloride. *Toxicol. Appl. Pharmacol.*, 177(2):112–120, Dec 2001.

[65] X. Volkmann, U. Fischer, M. J. Bahr, M. Ott, F. Lehner, M. Macfarlane, G. M. Cohen, M. P. Manns, K. Schulze-Osthoff, and H. Bantel. Increased hepatotoxicity of tumor necrosis factor-related apoptosis-inducing ligand in diseased human liver. *Hepatology*, 46(5):1498–1508, Nov 2007.

[66] J. P. Iredale. Hepatic stellate cell behavior during resolution of liver injury. *Semin. Liver Dis.*, 21(3):427–436, Aug 2001.

[67] T. M. Donohue. Alcohol-induced steatosis in liver cells. *World J. Gastroenterol.*, 13(37):4974–4978, Oct 2007.

[68] G. C. Farrell and C. Z. Larter. Nonalcoholic fatty liver disease: from steatosis to cirrhosis. *Hepatology*, 43(2 Suppl 1):S99–S112, Feb 2006.

[69] K. V. Menon, G. J. Gores, and V. H. Shah. Pathogenesis, diagnosis, and treatment of alcoholic liver disease. *Mayo Clin. Proc.*, 76(10):1021–1029, Oct 2001.

[70] C. S. Lieber and M. Savolainen. Ethanol and lipids. *Alcohol. Clin. Exp. Res.*, 8(4):409–423, 1984.

[71] J. E. Schaffer. Lipotoxicity: when tissues overeat. *Curr. Opin. Lipidol.*, 14(3):281–287, Jun 2003.

[72] J. A. Ibdah, H. Paul, Y. Zhao, S. Binford, K. Salleng, M. Cline, D. Matern, M. J. Bennett, P. Rinaldo, and A. W. Strauss. Lack of mitochondrial trifunctional protein in mice causes neonatal hypoglycemia and sudden death. *J. Clin. Invest.*, 107(11):1403–1409, Jun 2001.

[73] A. J. McCullough. Pathophysiology of nonalcoholic steatohepatitis. *J. Clin. Gastroenterol.*, 40 Suppl 1:17–29, Mar 2006.

[74] W. Bode and K. Maskos. Structural basis of the matrix metalloproteinases and their physiological inhibitors, the tissue inhibitors of metalloproteinases. *Biol. Chem.*, 384(6):863–872, Jun 2003.

[75] B. C. Jackson, D. W. Nebert, and V. Vasiliou. Update of human and mouse matrix metalloproteinase families. *Hum. Genomics*, 4(3):194–201, Feb 2010.

[76] R. Visse and H. Nagase. Matrix metalloproteinases and tissue inhibitors of metalloproteinases: structure, function, and biochemistry. *Circ. Res.*, 92(8):827–839, May 2003.

[77] R. T. Aimes and J. P. Quigley. Matrix metalloproteinase-2 is an interstitial collagenase. Inhibitor-free enzyme catalyzes the cleavage of collagen fibrils and soluble native type I collagen generating the specific 3/4- and 1/4-length fragments. *J. Biol. Chem.*, 270(11):5872–5876, Mar 1995.

[78] R. C. Benyon and M. J. Arthur. Extracellular matrix degradation and the role of hepatic stellate cells. *Semin. Liver Dis.*, 21(3):373–384, Aug 2001.

[79] P. A. Snoek-van Beurden and J. W. Von den Hoff. Zymographic techniques for the analysis of matrix metalloproteinases and their inhibitors. *BioTechniques*, 38(1):73–83, Jan 2005.

[80] Mmp9 matrix metallopeptidase 9 (gelatinase b, 92kda gelatinase, 92kda type iv collagenase) [homo sapiens (human)]. `http://www.ncbi.nlm.nih.gov/gene?Db=gene&Cmd=ShowDetailView&TermToSearch=4318`, 2013. [Online; accessed 22-April-2013].

[81] H. Yoshiji, S. Kuriyama, Y. Miyamoto, U. P. Thorgeirsson, D. E. Gomez, M. Kawata, J. Yoshii, Y. Ikenaka, R. Noguchi, H. Tsujinoue, T. Nakatani, S. S. Thorgeirsson, and H. Fukui. Tissue inhibitor of metalloproteinases-1 promotes liver fibrosis development in a transgenic mouse model. *Hepatology*, 32(6):1248–1254, Dec 2000.

[82] D. E. Gomez, D. F. Alonso, H. Yoshiji, and U. P. Thorgeirsson. Tissue inhibitors of metalloproteinases: structure, regulation and biological functions. *Eur. J. Cell Biol.*, 74(2):111–122, Oct 1997.

[83] W. Bode, C. Fernandez-Catalan, F. Grams, F. X. Gomis-Ruth, H. Nagase, H. Tschesche, and K. Maskos. Insights into MMP-TIMP interactions. *Ann. N. Y. Acad. Sci.*, 878:73–91, Jun 1999.

[84] B. K. Pilcher, M. Wang, X. J. Qin, W. C. Parks, R. M. Senior, and H. G. Welgus. Role of matrix metalloproteinases and their inhibition in cutaneous wound healing and allergic contact hypersensitivity. *Ann. N. Y. Acad. Sci.*, 878:12–24, Jun 1999.

[85] J. R. Chin and Z. Werb. Matrix metalloproteinases regulate morphogenesis, migration and remodeling of epithelium, tongue skeletal muscle and cartilage in the mandibular arch. *Development*, 124(8):1519–1530, Apr 1997.

[86] Mmp2 matrix metallopeptidase 2 (gelatinase a, 72kda gelatinase, 72kda type iv collagenase) [homo sapiens (human)]. `http://www.ncbi.nlm.nih.gov/gene/4313`, 2013. [Online; accessed 21-April-2013].

[87] M. M. Khan, S. Simizu, T. Suzuki, A. Masuda, M. Kawatani, M. Muroi, N. Dohmae, and H. Osada. Protein disulfide isomerase-mediated disulfide bonds regulate the gelatinolytic activity and secretion of matrix metalloproteinase-9. *Exp. Cell Res.*, 318(8):904–914, May 2012.

[88] J. Vandooren, P. E. Van den Steen, and G. Opdenakker. Biochemistry and molecular biology of gelatinase B or matrix metalloproteinase-9 (MMP-9): The next decade. *Crit. Rev. Biochem. Mol. Biol.*, Apr 2013.

[89] Wisconsin veterinary diagnostic laboratory. Real time pcr ct values. `www.wvdl.wisc.edu/pdf/wvdl.info.pcr_ct_values.pdf`. [Online; accessed 6-May-2013].

[90] A. Pellicoro, P. Ramachandran, and J. P. Iredale. Reversibility of liver fibrosis. *Fibrogenesis Tissue Repair*, 5 Suppl 1:S26, Jun 2012.

[91] R. Issa, X. Zhou, C. M. Constandinou, J. Fallowfield, H. Millward-Sadler, M. D. Gaca, E. Sands, I. Suliman, N. Trim, A. Knorr, M. J. Arthur, R. C. Benyon, and J. P. Iredale. Spontaneous recovery from micronodular cirrhosis: evidence for incomplete resolution associated with matrix cross-linking. *Gastroenterology*, 126(7):1795–1808, Jun 2004.

[92] M. J. Arthur. Reversibility of liver fibrosis and cirrhosis following treatment for hepatitis C. *Gastroenterology*, 122(5):1525–1528, May 2002.

[93] R. C. Benyon and J. P. Iredale. Is liver fibrosis reversible? *Gut*, 46(4):443–446, Apr 2000.

[94] R. Bataller and D. A. Brenner. Hepatic stellate cells as a target for the treatment of liver fibrosis. *Semin. Liver Dis.*, 21(3):437–451, Aug 2001.

[95] P. Ramachandran and J. P. Iredale. Reversibility of liver fibrosis. *Ann Hepatol*, 8(4):283–291, 2009.

[96] G. Tan, S. Pan, J. Li, X. Dong, K. Kang, M. Zhao, X. Jiang, J. R. Kanwar, H. Qiao, H. Jiang, and X. Sun. Hydrogen sulfide attenuates carbon tetrachloride-induced hepatotoxicity, liver cirrhosis and portal hypertension in rats. *PLoS ONE*, 6(10):e25943, 2011.

[97] L. Fang, H. Li, C. Tang, B. Geng, Y. Qi, and X. Liu. Hydrogen sulfide attenuates the pathogenesis of pulmonary fibrosis induced by bleomycin in rats. *Can. J. Physiol. Pharmacol.*, 87(7):531–538, Jul 2009.

[98] E. Lowicka and J. Beltowski. Hydrogen sulfide (H2S) - the third gas of interest for pharmacologists. *Pharmacol Rep*, 59(1):4–24, Feb 2007.

[99] R. Hosoki, N. Matsuki, and H. Kimura. The possible role of hydrogen sulfide as an endogenous smooth muscle relaxant in synergy with nitric oxide. *Biochem. Biophys. Res. Commun.*, 237(3):527–531, Aug 1997.

[100] Z. Fu, X. Liu, B. Geng, L. Fang, and C. Tang. Hydrogen sulfide protects rat lung from ischemia-reperfusion injury. *Life Sci.*, 82(23-24):1196–1202, Jun 2008.

[101] Animal care Boston university reseach compliance. Intraperitoneal injection. `http://www.bu.edu/animalcare/procedures/injection-techniques/intraperitoneal/`. [Online; accessed 6-May-2013].

[102] C. Wang, H. Y. Wang, Z. W. Liu, Y. Fu, and B. Zhao. Effect of endogenous hydrogen sulfide on oxidative stress in oleic acid-induced acute lung injury in rats. *Chin. Med. J.*, 124(21):3476–3480, Nov 2011.

[103] Y. Liu, C. Meyer, C. Xu, H. Weng, C. Hellerbrand, P. ten Dijke, and S. Dooley. Animal models of chronic liver diseases. *Am. J. Physiol. Gastrointest. Liver Physiol.*, 304(5):G449–468, Mar 2013.

[104] H. Hayashi and T. Sakai. Animal models for the study of liver fibrosis: new insights from knockout mouse models. *Am. J. Physiol. Gastrointest. Liver Physiol.*, 300(5):G729–738, May 2011.

[105] C. Constandinou, N. Henderson, and J. P. Iredale. Modeling liver fibrosis in rodents. *Methods Mol. Med.*, 117:237–250, 2005.

[106] Y. Jiang, J. Liu, M. Waalkes, and Y. J. Kang. Changes in the gene expression associated with carbon tetrachloride-induced liver fibrosis persist after cessation of dosing in mice. *Toxicol. Sci.*, 79(2):404–410, Jun 2004.

[107] P. Mayoral, M. Criado, F. Hidalgo, O. Flores, M. A. Arevalo, N. Eleno, A. Sanchez-Rodriguez, J. M. Lopez-Novoa, and A. Esteller. Effects of chronic nitric oxide activation or inhibition on early hepatic fibrosis in rats with bile duct ligation. *Clin. Sci.*, 96(3):297–305, Mar 1999.

[108] J. M. Dwyer and C. Johnson. The use of concanavalin A to study the immunoregulation of human T cells. *Clin. Exp. Immunol.*, 46(2):237–249, Nov 1981.

[109] H. Ehlken, V. Kondylis, J. Heinrichsdorff, L. Ochoa-Callejero, T. Roskams, and M. Pasparakis. Hepatocyte IKK2 protects Mdr2-/- mice from chronic liver failure. *PLoS ONE*, 6(10):e25942, 2011.

[110] M. Varela-Rey, N. Martinez-Lopez, D. Fernandez-Ramos, N. Embade, D. F. Calvisi, A. Woodhoo, J. Rodriguez, M. F. Fraga, J. Julve, E. Rodriguez-Millan, I. Frades, L. Torres, Z. Luka, C. Wagner, M. Esteller, S. C. Lu, M. L. Martinez-Chantar, and J. M. Mato. Fatty liver and fibrosis in glycine N-methyltransferase knockout mice is prevented by nicotinamide. *Hepatology*, 52(1):105–114, Jul 2010.

[111] chromosome 1 open reading frame 85. `http://www.genecards.org/cgi-bin/carddisp.pl?gene=C1orf85`. [Online; accessed 26-May-2013].

[112] K. R. Steffensen, M. Bouzga, F. Skjeldal, C. Kasi, A. Karahasan, V. Matre, O. Bakke, S. Guerin, and W. Eskild. Human NCU-G1 can function as a transcription factor and as a nuclear receptor co-activator. *BMC Mol. Biol.*, 8:106, 2007.

[113] O. Schieweck, M. Damme, B. Schroder, A. Hasilik, B. Schmidt, and T. Lubke. NCU-G1 is a highly glycosylated integral membrane protein of the lysosome. *Biochem. J.*, 422(1):83–90, Aug 2009.

[114] T. Aoyama, J. M. Peters, N. Iritani, T. Nakajima, K. Furihata, T. Hashimoto, and F. J. Gonzalez. Altered constitutive expression of

fatty acid-metabolizing enzymes in mice lacking the peroxisome proliferator-activated receptor alpha (PPARalpha). *J. Biol. Chem.*, 273(10):5678–5684, Mar 1998.

[115] X. Y. Kong, C. K. Nesset, M Damme, Lberg E. M., T. Lbke, J. Mhlen, K. B. Andersson, P. I. Lorenzo, N. Roos, Thoresen G. H., A. Rustan, E. T. Kase, and W. Eskild. Spontaneous liver fibrosis in mice due to lack of NCU-G1. *Submitted.*, 2013.

[116] T. Lubke, P. Lobel, and D. E. Sleat. Proteomics of the lysosome. *Biochim. Biophys. Acta*, 1793(4):625–635, Apr 2009.

[117] L. E. Karageorgos, E. L. Isaac, D. A. Brooks, E. M. Ravenscroft, R. Davey, J. J. Hopwood, and P. J. Meikle. Lysosomal biogenesis in lysosomal storage disorders. *Exp. Cell Res.*, 234(1):85–97, Jul 1997.

[118] M. L. Schultz, L. Tecedor, M. Chang, and B. L. Davidson. Clarifying lysosomal storage diseases. *Trends Neurosci.*, 34(8):401–410, Aug 2011.

[119] A. P. Lieberman, R. Puertollano, N. Raben, S. Slaugenhaupt, S. U. Walkley, and A. Ballabio. Autophagy in lysosomal storage disorders. *Autophagy*, 8(5):719–730, May 2012.

[120] K. Schopfer, E. Miebach, M. Beck, and S. Pitz. [Lysosomal storage diseases - update and new therapeutic options]. *Klin Monbl Augenheilkd*, 228(2):144–160, Feb 2011.

[121] Lysosomal storage disease. `http://emedicine.medscape.com/article/1182830-overview`, 2011. [Online; accessed 2-May-2013].

[122] T.A. Burrow, K.E. Bove, and G.A. Grabowski. *Liver Disease in Children.* University Publishing Online, 2007.

[123] G. A. Grabowski and R. J. Hopkin. Enzyme therapy for lysosomal storage disease: principles, practice, and prospects. *Annu Rev Genomics Hum Genet*, 4:403–436, 2003.

[124] T. Kurz, A. Terman, B. Gustafsson, and U. T. Brunk. Lysosomes and oxidative stress in aging and apoptosis. *Biochim. Biophys. Acta*, 1780(11):1291–1303, Nov 2008.

[125] R. H. Lachmann, D. G. Wight, D. J. Lomas, N. C. Fisher, J. P. Schofield, E. Elias, and T. M. Cox. Massive hepatic fibrosis in Gaucher's disease: clinico-pathological and radiological features. *QJM*, 93(4):237–244, Apr 2000.

[126] N. L. Sayre, V. M. Rimkunas, M. J. Graham, R. M. Crooke, and L. Liscum. Recovery from liver disease in a Niemann-Pick type C mouse model. *J. Lipid Res.*, 51(8):2372–2383, Aug 2010.

[127] T. M. Cox and J. P. Schofield. Gaucher's disease: clinical features and natural history. *Baillieres Clin. Haematol.*, 10(4):657–689, Dec 1997.

[128] C. Putterman, J. Zelingher, and D. Shouval. Liver failure and the sea-blue histiocyte/adult Niemann-Pick disease. Case report and review of the literature. *J. Clin. Gastroenterol.*, 15(2):146–149, Sep 1992.

[129] C. Settembre, A. Fraldi, D. C. Rubinsztein, and A. Ballabio. Lysosomal storage diseases as disorders of autophagy. *Autophagy*, 4(1):113–114, Jan 2008.

[130] J. S. Kim, T. Nitta, D. Mohuczy, K. A. O'Malley, L. L. Moldawer, W. A. Dunn, and K. E. Behrns. Impaired autophagy: A mechanism of mitochondrial dysfunction in anoxic rat hepatocytes. *Hepatology*, 47(5):1725–1736, May 2008.

[131] QIAGEN. Rneasy® plus universal handbook. `http://www.qiagen.com/resources/download.asp`. [Online; accessed 24-February-2013].

[132] Thermo scientific. 009technical bulletin, nanodrop 1000 & 8000, 260/280 and 260/230 ratios. `www.nanodrop.com`. [Online; accessed 24-February-2013].

[133] B. Alberts, A. Johnson, J. Lewis, M. Raff, K. Roberts, and P. Walter. *Molecular Biology of THE CELL*. Garland Science, 5. edition, 2008.

[134] Roche. Transcriptor first strand cdna syntesis kit manual. `cssportal.roche.com`. [Online; accessed 25-February-2013].

[135] Roche. Lightcycler 480 dna sybr green i master manual. `www.cbmg.umd.edu`. [Online; accessed 25-February-2013].

[136] I. Rieu and S. J. Powers. Real-time quantitative RT-PCR: design, calculations, and statistics. *Plant Cell*, 21(4):1031–1033, Apr 2009.

[137] E. Eisenberg and E. Y. Levanon. Human housekeeping genes are compact. *Trends Genet.*, 19(7):362–365, Jul 2003.

[138] PREMIER Biosoft. Pcr primer design guidelines. `http://www.premierbiosoft.com/tech_notes/PCR_Primer_Design.html`. [Online; accessed 14-May-2013].

[139] Bio-Rad. Bio-rad protein assay manual. `labs.fhcrc.org`. [Online; accessed 25-February-2013].

[140] K. L. Gorres and R. T. Raines. Prolyl 4-hydroxylase. *Crit. Rev. Biochem. Mol. Biol.*, 45(2):106–124, Apr 2010.

[141] Quickzyme. Hydroxyproline assay manual. `www.QuickZyme.com`. [Online; accessed 25-February-2013].

[142] Mysid/PD. Hydroxyproline chemical structure. `http://chemistry.about.com/od/factsstructures/ig/Chemical-Structures---H/Hydroxyproline.htm`. [Online; accessed 14-May-2013].

[143] The Faculty of Mathematics University of Oslo: Department of Biosciences and Natural Sciences. Sds-polyakrylamid gel electrophoresis. `http://www.mn.uio.no/ibv/tjenester/kunnskap/plantefys/leksikon/s/sds.html`. [Online; accessed 14-May-2013].

[144] Western blotting handbook and troubleshooting guide. `http://www.piercenet.com/Objects/View.cfm`, 2004. [Online; accessed 22-May-2013].

[145] GE Healtcare life sciences. Amersham ecl plus western blotting detection reagents. `www.gelifesciences.com`. [Online; accessed 25-February-2013].

[146] Thermo scientific. Strip and reprobe western blots. `www.piercenet.com/files/TR0023-strip-and-reprobe-blots.pdf`. [Online; accessed 15-May-2013].

[147] L. Troeberg and H. Nagase. Zymography of metalloproteinases. *Curr Protoc Protein Sci*, Chapter 21:Unit 21.15, Nov 2004.

[148] Special Diets Services (SDS). Rat and mouse no.1 maintenance; pelleted, expanded and expanded ground. http://www.nova-scb.com/fileadmin/Scanbur_Research_Consumables/Agentur/SDS/RM1_P__E__FG_.pdf. [Online; accessed 27-February-2013].

[149] S100a8 s100 calcium binding protein a8 [homo sapiens (human)]. http://www.ncbi.nlm.nih.gov/gene?cmd=Retrieve&dopt=full_report&list_uids=6279, 2008. [Online; accessed 22-April-2013].

[150] N. Mizushima and T. Yoshimori. How to interpret LC3 immunoblotting. *Autophagy*, 3(6):542–545, 2007.

[151] Y. Kabeya, N. Mizushima, T. Ueno, A. Yamamoto, T. Kirisako, T. Noda, E. Kominami, Y. Ohsumi, and T. Yoshimori. LC3, a mammalian homologue of yeast Apg8p, is localized in autophagosome membranes after processing. *EMBO J.*, 19(21):5720–5728, Nov 2000.

[152] A. Fawcett. Guidelines for the housing of mice in scientific institutions. http://www.animalethics.org.au/__data/assets/pdf_file/0004/249898/Guideline-22-mouse-housing.pdf, 2012. [Online; accessed 17-April-2013].

[153] P. G. Martin, H. Guillou, F. Lasserre, S. Dejean, A. Lan, J. M. Pascussi, M. Sancristobal, P. Legrand, P. Besse, and T. Pineau. Novel aspects of PPARalpha-mediated regulation of lipid and xenobiotic metabolism revealed through a nutrigenomic study. *Hepatology*, 45(3):767–777, Mar 2007.

[154] Y. S. Seo, J. H. Kim, N. Y. Jo, K. M. Choi, S. H. Baik, J. J. Park, J. S. Kim, K. S. Byun, Y. T. Bak, C. H. Lee, A. Kim, and J. E. Yeon. PPAR agonists treatment is effective in a nonalcoholic fatty liver disease animal model by modulating fatty-acid metabolic enzymes. *J. Gastroenterol. Hepatol.*, 23(1):102–109, Jan 2008.

[155] M. Bolognesi, C. Merkel, D. Sacerdoti, V. Nava, and A. Gatta. Role of spleen enlargement in cirrhosis with portal hypertension. *Dig Liver Dis*, 34(2):144–150, Feb 2002.

[156] R. Domitrovic, H. Jakovac, J. Tomac, and I. Sain. Liver fibrosis in mice induced by carbon tetrachloride and its reversion by luteolin. *Toxicol. Appl. Pharmacol.*, 241(3):311–321, Dec 2009.

[157] M. R. Ebrahimkhani, S. Kiani, F. Oakley, T. Kendall, A. Shariftabrizi, S. M. Tavangar, L. Moezi, S. Payabvash, A. Karoon, H. Hoseininik, D. A. Mann, K. P. Moore, A. R. Mani, and A. R. Dehpour. Naltrexone, an opioid receptor antagonist, attenuates liver fibrosis in bile duct ligated rats. *Gut*, 55(11):1606–1616, Nov 2006.

[158] T. Takehara, T. Tatsumi, T. Suzuki, E. B. Rucker, L. Hennighausen, M. Jinushi, T. Miyagi, Y. Kanazawa, and N. Hayashi. Hepatocyte-specific disruption of Bcl-xL leads to continuous hepatocyte apoptosis and liver fibrotic responses. *Gastroenterology*, 127(4):1189–1197, Oct 2004.

[159] H. S. Lee, C. T. Shun, L. L. Chiou, C. H. Chen, G. T. Huang, and J. C. Sheu. Hydroxyproline content of needle biopsies as an objective measure of liver fibrosis: Emphasis on sampling variability. *J. Gastroenterol. Hepatol.*, 20(7):1109–1114, Jul 2005.

[160] A. T. Gomes, C. G. Bastos, C. L. Afonso, B. F. Medrado, and Z. A. Andrade. How variable are hydroxyproline determinations made in different samples of the same liver? *Clin. Biochem.*, 39(12):1160–1163, Dec 2006.

[161] J. P. Iredale, R. C. Benyon, J. Pickering, M. McCullen, M. Northrop, S. Pawley, C. Hovell, and M. J. Arthur. Mechanisms of spontaneous resolution of rat liver fibrosis. Hepatic stellate cell apoptosis and reduced hepatic expression of metalloproteinase inhibitors. *J. Clin. Invest.*, 102(3):538–549, Aug 1998.

[162] Y. Z. Tu, J. Zhang, H. P. Liu, and W. Yu. [Inhibition of liver fibrosis by IL-10 gene-modified BMSCs in a rat model]. *Zhonghua Gan Zang Bing Za Zhi*, 20(12):908–911, Dec 2012.

[163] Y. Popov, E. Patsenker, P. Fickert, M. Trauner, and D. Schuppan. Mdr2 (Abcb4)-/- mice spontaneously develop severe biliary fibrosis via massive dysregulation of pro- and antifibrogenic genes. *J. Hepatol.*, 43(6):1045–1054, Dec 2005.

[164] J. Varga and S. A. Jimenez. Stimulation of normal human fibroblast collagen production and processing by transforming growth factor-beta. *Biochem. Biophys. Res. Commun.*, 138(2):974–980, Jul 1986.

[165] C. M. Overall, J. L. Wrana, and J. Sodek. Independent regulation of collagenase, 72-kDa progelatinase, and metalloendoproteinase inhibitor expression in human fibroblasts by transforming growth factor-beta. *J. Biol. Chem.*, 264(3):1860–1869, Jan 1989.

[166] H. Herbst, T. Wege, S. Milani, G. Pellegrini, H. D. Orzechowski, W. O. Bechstein, P. Neuhaus, A. M. Gressner, and D. Schuppan. Tissue inhibitor of metalloproteinase-1 and -2 RNA expression in rat and human liver fibrosis. *Am. J. Pathol.*, 150(5):1647–1659, May 1997.

[167] Q. Yu and I. Stamenkovic. Cell surface-localized matrix metalloproteinase-9 proteolytically activates TGF-beta and promotes tumor invasion and angiogenesis. *Genes Dev.*, 14(2):163–176, Jan 2000.

[168] N. Akpolat, S. Yahsi, A. Godekmerdan, M. Yalniz, and K. Demirbag. The value of alpha-SMA in the evaluation of hepatic fibrosis severity in hepatitis B infection and cirrhosis development: a histopathological and immunohistochemical study. *Histopathology*, 47(3):276–280, Sep 2005.

[169] A. Desmouliere, A. Geinoz, F. Gabbiani, and G. Gabbiani. Transforming growth factor-beta 1 induces alpha-smooth muscle actin expression in granulation tissue myofibroblasts and in quiescent and growing cultured fibroblasts. *J. Cell Biol.*, 122(1):103–111, Jul 1993.

[170] E. R. Garcia-Trevijano, M. J. Iraburu, L. Fontana, J. A. Dominguez-Rosales, A. Auster, A. Covarrubias-Pinedo, and M. Rojkind. Transforming growth factor beta1 induces the expression of alpha1(I) procollagen mRNA by a hydrogen peroxide-C/EBPbeta-dependent mechanism in rat hepatic stellate cells. *Hepatology*, 29(3):960–970, Mar 1999.

[171] C. Ryckman, K. Vandal, P. Rouleau, M. Talbot, and P. A. Tessier. Proinflammatory activities of S100: proteins S100A8, S100A9, and S100A8/A9 induce neutrophil chemotaxis and adhesion. *J. Immunol.*, 170(6):3233–3242, Mar 2003.

[172] W. Nacken, J. Roth, C. Sorg, and C. Kerkhoff. S100A9/S100A8: Myeloid representatives of the S100 protein family as prominent players in innate immunity. *Microsc. Res. Tech.*, 60(6):569–580, Apr 2003.

[173] R. J. Passey, K. Xu, D. A. Hume, and C. L. Geczy. S100A8: emerging functions and regulation. *J. Leukoc. Biol.*, 66(4):549–556, Oct 1999.

[174] K. Brew, D. Dinakarpandian, and H. Nagase. Tissue inhibitors of metalloproteinases: evolution, structure and function. *Biochim. Biophys. Acta*, 1477(1-2):267–283, Mar 2000.

[175] D. E. Kleiner and W. G. Stetler-Stevenson. Quantitative zymography: detection of picogram quantities of gelatinases. *Anal. Biochem.*, 218(2):325–329, May 1994.

[176] F. R. Murphy, R. Issa, X. Zhou, S. Ratnarajah, H. Nagase, M. J. Arthur, C. Benyon, and J. P. Iredale. Inhibition of apoptosis of activated hepatic stellate cells by tissue inhibitor of metalloproteinase-1 is mediated via effects on matrix metalloproteinase inhibition: implications for reversibility of liver fibrosis. *J. Biol. Chem.*, 277(13):11069–11076, Mar 2002.

[177] G. Opdenakker, P. E. Van den Steen, and J. Van Damme. Gelatinase B: a tuner and amplifier of immune functions. *Trends Immunol.*, 22(10):571–579, Oct 2001.

[178] H. N. Fan, H. J. Wang, C. R. Yang-Dan, L. Ren, C. Wang, Y. F. Li, and Y. Deng. Protective effects of hydrogen sulfide on oxidative stress and fibrosis in hepatic stellate cells. *Mol Med Rep*, Oct 2012.

[179] H. N. Fan, H. J. Wang, L. Ren, B. Ren, C. R. Dan, Y. F. Li, L. Z. Hou, and Y. Deng. Decreased expression of p38 MAPK mediates protective effects of hydrogen sulfide on hepatic fibrosis. *Eur Rev Med Pharmacol Sci*, 17(5):644–652, Mar 2013.

[180] C. Settembre, A. Fraldi, L. Jahreiss, C. Spampanato, C. Venturi, D. Medina, R. de Pablo, C. Tacchetti, D. C. Rubinsztein, and A. Ballabio. A block of autophagy in lysosomal storage disorders. *Hum. Mol. Genet.*, 17(1):119–129, Jan 2008.

Appendix A

Materials

A.1 Primers

Table A.1: **Primers used for genotyping:**

Primer name	**5'-Primer**	**3'-Primer**	**Expected product size**
Gene-trap	GATGTCAAGAAGAGACGTTGGGTT	GCATCGCATTGTCTGAGTAGGTGT	811bp
Ncug1	GGAGAAGAGACTCGCCAGGTAAGG	GCTGCCCACTGCCCGAATA	562bp

Table A.2: **Primers used in real-time qRT-PCR:**

Target gene	**Description**	**5'-Primer**	**3'-Primer**
MMP-2	Matrix metallopeptidase 2	TGATAACCTGGATGCCGTCGT	TGCTTCCAAACTTCACGCTCT
MMP-9	Matrix metallopeptidase 9	CTTTGAGTCCGGCAGACAAT	TTCCAGTACCAACCGTCCTT
TIMP1	Tissue inhibitor of metalloproteinases 1	GGCATCCTCTTGTTGCTATCACT	CTTATGACCAGGTCCGAGTTGC
S100A8	S100 calcium binding protein A8	CCGTCTTCAAGACATCGTTTGA	GTAGAGGGCATGGTGATTTCCT
TGF-β1	Transforming growth factor β1	GCACCATCCATGACATGAACC	AAGTCAATGTACAGCTGCCGC
α-SMA	Alpha-smooth muscle actin	CCACCGCAAATGCTTCTAAGT	GGCAGGAATGATTTGGAAAGG
Col1α1	Collagen, type I, alpha 1	GCTTCACCTACAGCACCCTTGTGG	GAGGGAGTTTACACGAAGCAGGCAG
eEF2	Eukaryotic translation elongation factor 2	CCATCGCTGAACGCATCAAG	CAGGCCAGAACCAAAGCCTA

A.2 Protein gels

Table A.3: **Protein gels:**

Gel	**Manufacturer**
NuPAGE® Novex® 10% Bis-Tris Gels, 1.0 mm, 12 well	Life Tech
Novex® 10% Zymogram (Gelatin) Gel 1.0 mm, 12 Well.	Life Tech

A.3 Antibodies

Table A.4: **Antibodies:**

	Antibody	**Product size**	**Dilution**	**Manufacturer**
Primary antibodies	Rabbit-anti LC3	16 + 14 kDa	1:1000	Cell Signaling
	Goat-anti β-actin	42 kDa	1:5000	Abcam
Secondary antibodies	HRP-Goat-anti-Rabbit		1:4000	Zymed
	HRP-Donkey-anti-Goat		1:5000	Santa Cruz Biotechnology

A.4 Kits

Table A.5: **Kits:**

Name	**Manufacturer**
RNeasy Plus Mini Kit	Qiagen
Fastprep-24 lysing matrix tubes	MP
Transcriptor first strand cDNA syntesis kit	Roche
LightCycler 480 DNA SYBR Green I Master	Roche
Hydroxyproline kit	QuickZyme
Amershan ECL Plus Western Blotting Detection system	GE Healthcare

A.5 Chemicals

Agarose	Lonza
β-Mercaptoethanol (98%)	Sigma
Bio-Safe^{TM} Coomassie G250 stain	BioRad
Bovine serum albumine	Sigma
Brij 35	Santa Cruz Biotechnology
Bromphenol blue (bpb)	Sigma
Calcium chloride ($CaCl_2$)	Sigma
Coomassie Blue R250 stain	Invitrogen
Dithiothreitol (DTT)	Roche
Dynazyme (Tac-polymerase)	Sigma
Ethanol (EtOH)	Arcus
Ethidium bromide	Sigma
Ethylenediaminetetraacetic acid (EDTA)	Appli Chem
Fluanison (Hypnorm)	Roche
Genotyping MX buffer	Sigma-Aldrich
Glycerol	Merck
Hydrochloric acid (HCl)	Sigma
Isopropyl alcohol	Arcus
Methanol	Sigma
Midazolam (Dormicum)	Roche
MOPS buffer	Invitrogen
NP-40 (aka IGEPAL)	Sigma
NuPAGE LDS sample	Invitrogen
NuPAGE reducing agent	Invitrogen
Potassium chloride (KCl)	Merck
Potassium hydrogen phosphate (KH_2PO_4)	Merck
Protein Assay dye reagent	BioRad
Proteinase inhibitor mix	Sigma
Proteinase K	Thermo Scientific
RNAlater® Solution	Ambion
Sea Kem® LE Agarose	Lonza
Simply Blue^{TM}	Invitrogen
Skim milk powder	Fluka analytical

Sodium chloride (NaCl)	VWR
Sodium dodecyl sulfate (SDS)	Sigma
Sodium hydrosulfide (NaHS)	Santa Cruz Biotechnology
Sodium hydroxide (NaOH)	SDS
Sodium orthovanadate (Na_3VO_4)	Sigma
Sodium phosphate ($NaHPO_4$)	Merck
Tris-base	Merck
Tris-HCl	VWR
Triton x100	Sigma
Tween 20	Sigma

Appendix B

Solutions

Table B.1: **Lysis buffer:**

TrisHCL pH7.4 @ RT	50 mM
EDTA	5 mM
Sodium Orthovanadate	1 mM
NP-40 (aka IGEPAL)	0.2%
Triton X-100	0.1%
Protease inhibitor mix	10 μl

Table B.2: **Sample buffer for SDS-gel electrophoresis (5X):**

Tris-HCl (pH 6.8, 0.225M)	2.25 ml	1 M
Glycerol (50%)	5 ml	
SDS (5%)	0.5 g	
bpb (0.05%)	5 mg	
DTT (0.25M)	2.5 ml	1 M
Total volume	10 ml	

Table B.3: **Blotting buffer:**

Tris base	15 g
Glycine	72.5 g
Methanol	1 l
Add MQ water to total volume	5 l

Table B.4: **TBS buffer (10X)** (pH 7.6):

Tris base	24 g
NaCl	88 g
HCl	(adjust pH to 7.6)
Add MQ water to total volume	1 l

Table B.5: **TBS buffer with 0.1% Tween:**

10xTBS buffer	50 ml
MQ water	450 ml
Tween 20	0.5 ml
Total volume	500 ml

Table B.6: **Zymography sample buffer (2X):**

0.5 M Tris-HCl, pH 6.8	3.5 ml
Glycerol	2.0 ml
10% (w/v) SDS	4.0 ml
0.1% Bromophenol Blue	0.5 ml
Water	1.0 ml
Total volume	10 ml

Table B.7: **Zymography running buffer (10X) (pH 8.3):**

Tris Base	29 g
Glycine	144 g
SDS	10 g
Solve in water to volume	1 l

Table B.8: **Zymography renaturing buffer (10X):**

Triton X-100	2.5 ml
MQ water	7.5 ml

Table B.9: **Zymography Developing buffer (10X):**

Tris Base	12.1 g
Tris-HCl	63.0 g
NaCl	117 g
$CaCl_2$	7.4 g
Brij 35	0.2%
Solve in MQ water to volume	1 l

Table B.10: **PBS buffer:**

NaCl	80 g
KCl	2 g
Na_2HPO_4	14.4 g
KH_2PO_4	2.4 g
HCl	(adjust pH to 7.4)
Solve in MQ water to volume	1 l

Table B.11: **NaHS solution:**

NaHS	100 mg
solve in PBS buffer to total volume	10 ml

Table B.12: **Genotyping Lysis buffer:**

Tris-HCl (pH 8.5, 1M)	50 ml	100 mM
EDTA (0.5M)	5 ml	2 mM
SDS (10%)	10 ml	0.2%
NaCl (5M)	20 ml	200 mM
Solve in Milli Q H2O to volume	500 ml	
Solve in water to volume	1 l	

Table B.13: **Agarose gel (1%)** (100ml for big gel with two combs):

1xTae buffer	100 ml
Agarose	1 g
EtBr (2.5 mg/ml)	24 μl

Appendix C

Standards

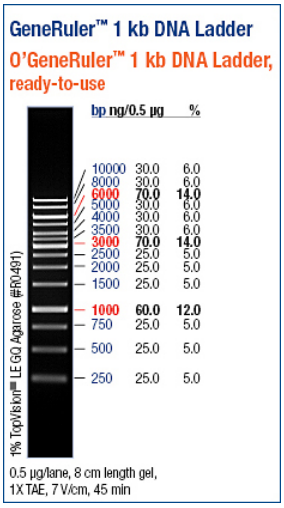

Figure C.1: **GeneRuler^{TM} 1 kb DNA Ladder (SM0312)** Thermo scientific.

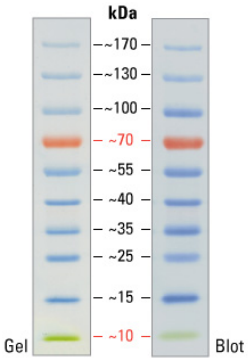

Figure C.2: **PageRuler^{TM} Prestained Protein Ladder, (SM0671)** Fermentas.

Appendix D

Supplementary figures

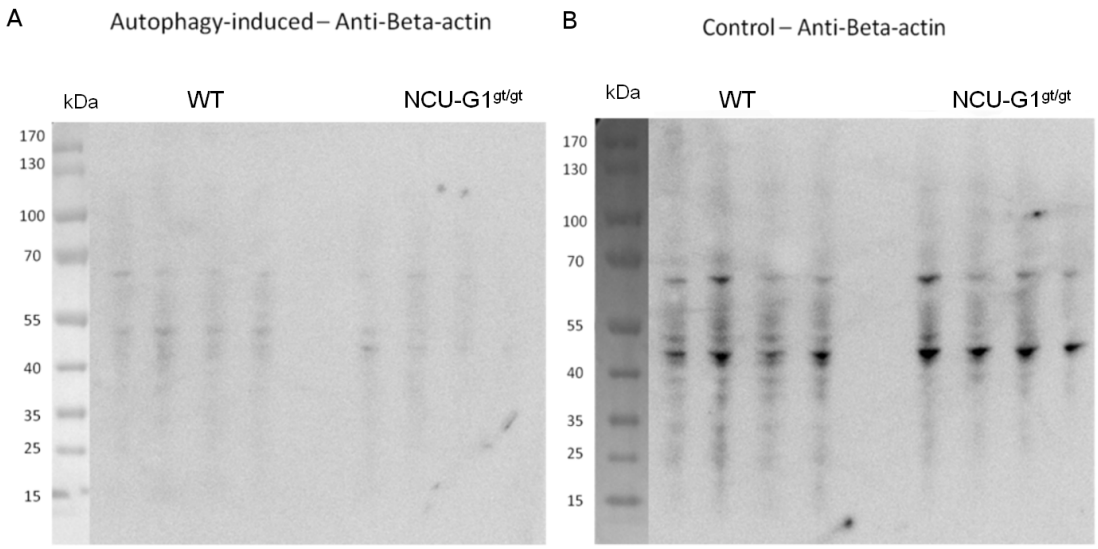

Supplementary Figure D.1: **Detection of β-actin as housekeeping protein for Western blot analysis.** The Western blot membrane used for analysis of autophagy marker LC3 in 4.5 months old *NCU-G1$^{gt/gt}$* and WT mice livers were analysed with β-actin antibodies after stripping of the membrane. **(A)** Autophagy induced and **(B)** control, *NCU-G1$^{gt/gt}$* and WT mice, liver samples (n=4) were investigated for the presence of β-actin with a band size of 42 kDa.